Electronic Supplementary Material (ESI) for Energy & Environmental Science.

Water-based layer-by-layer processing enables 19 % efficient binary organic solar cells with minimized thickness sensitivity

Experimental section

Materials: PM6 (Mn = 45,000, Mw = 97,000), BTP-eC9, L8-BO-F were purchased from Solarmer Materials Inc. CTAB and SDS and all the solvents were purchased from Sigma-Aldrich and used as received.

Nanoparticle preparation: Donor polymers 5 mg were dissolved in 1mL chloroform and stirred at 50 °C for 3h. Then the solution was added to 10 mL 10 mg mL^{-1} CTAB or SDS aqueous solution and stirred at 40 °C for 1h. The formed micro-emulsion dispersion was ultrasonicated using a SCIENTZ-IID ultrasonic finger (200 watt, 5 min) in a ice-water bath. The miniemulsion system was heated at 40 °C while constant stirring until chloroform was completely eliminated. The excess surfactant from the particle solution was removed using Amicon® ultra-15 centrifuge filter (cutoff 30K). The dispersion was placed into the filter and centrifuged at 4000 rpm for 20 min. The retentate was raised to 15 mL with water and then centrifuged again. This process was repeated for 5 several times until surface tension of the filtrate reached 38 ± 2 mN m^{-1}. The retentate was filtered by a 0.45 μm filter before the last centrifugation.

Solar cells fabrication and characterization: Solar cell devices were fabricated in the conventional structure of ITO/PEDOT: PSS/Active layer/PNDIT-F3N/Ag. The pre-structured ITO/glass or ITO/PET were cleaned with acetone and isopropyl alcohol in an ultrasonic bath for 10 min each. After drying, the substrates were coated with 30 nm of PEDOT:PSS (CLEVIOS TM P VP Al 4083) by spin-coating at 5000 rpm and annealed at 150 °C for 15 min. For BHJ devices processed by o-xylene, the active layer PM6:BTP-eC9 solution with polymer concentration of 8 mg mL^{-1} (D:A = 1:1.2, 0.5% DIO) was spin-coated on PEDOT:PSS at 4000 rpm. For LBL devices, a 10 mg mL^{-1} PM6 o-xylene solution was firstly deposited at 1800 rpm on PEDOT:PSS, followed by deposing 8 mg mL^{-1} BTP-eC9 solution at 2000 rpm. Before active layer-processing in mn-LBL devices, pure toluene was spin-rinsed on PEDOT:PSS layer. Then an aqueous donor NP ink of 20 mg mL^{-1} was spin-coated onto a heated PEDOT:PSS substrate (80 °C) at 1250 rpm for 1 min in air. To remove remaining surfactant, the substrate was spin-rinsed with pure ethanol at 2000 rpm for 3 times. Then the substrate was immediately placed into a N_2-filled glovebox and stored overnight. After thermal annealing, the BTP-eC9 or BTP-eC9 with 30% DTT (weight ratio relative to BTP-eC9) solution of 8 mg mL^{-1} in o-xylene was spin-coated at 2000 rpm. The substrate was then annealed at 100 °C for 5 min.

To be detailed, for thick mn-LBL devices, the 250 nm and 400 nm thickness were given by aqueous PM6 ink of 40 mg mL^{-1} and 80 mg mL^{-1}, respectively. The concentration of acceptor was 15 mg mL^{-1} for 250 nm and 20 mg mL^{-1} for 400 nm film, respectively. For other solvents processed PM6:BTP-eC9 devices, the chloroform solution of PM6 was fixed to 7 mg mL^{-1}. The concentration for chloroform solution of BTP-eC9 is 7 mg mL^{-1} and 10 mg mL^{-1} for toluene, THF, Me-THF and DCM. The mn-PM6 layers in CF and toluene processed devices were annealed at 100 °C and the annealing temperature was 80 °C for devices processed by THF, Me-THF and DCM.

After active layer deposition, a 0.5 mg mL^{-1} methanol solution of PNDIT-F3N was deposited at 3000 rpm for 30s in nitrogen atmosphere, followed by thermal evaporation of 100 nm of silver through a shadow mask with a 6 mm^2 active area opening under a vacuum of approximately 1×10^{-6} mbar. The current–voltage characteristics of the solar cells were measured under AM 1.5 G irradiation on a Newport solar simulator (Taiwan, China). The light source was calibrated using a silicon reference cell. All the cells were tested under an inert atmosphere. EQEs were measured using an Enlitech QE−S EQE system (Taiwan, China) that was equipped with a standard Si diode. Monochromatic light was generated from a Newport 300 W lamp source. The photo-stability of the solar cells was performed under continuous one-sun illumination from a LED light (wavelength ranges from 400 to 800 nm) in a home-built chamber filled with N_2. Single carrier devices were fabricated and the dark J–V characteristics measured and analyzed in the SCL regime following the references. The architecture of hole-only devices was glass/ITO/PEDOT:PSS (30 nm)/active layer/MoO_x (10 nm)/Ag (100 nm). The architecture of electron-only devices was glass/ITO/ZnO (30 nm)/active layer/Ca (5 nm)/Ag (100 nm). The reported mobility data are average values over the 18 devices of each sample for a range of thicknesses. The SCLC curves can be fit to the Mott–Gurney relation for SCLC:[1]

$$J_{SCL} = \frac{9}{8}\varepsilon_0\varepsilon_r\mu\frac{V_{in}^2}{L^3}exp\left(\frac{0.89\beta}{L^{0.5}}V_{in}^{0.5}\right) \quad (1)$$

where J_{SCL} is the current density, $\varepsilon_0\varepsilon_r$ is the dielectric permittivity, μ is the carrier mobility, L is the film device, and β is the field activation factor.[2]

TPV and TPC were investigated by a TranPVC setup from Oriental Spectra Technology (Guangzhou, China) Co., Ltd.

Characterization of optical properties: Particle size and distribution were determined by dynamic light scattering (DLS) using a Malvern Zetasizer Nano ZS90 from Malvern Panalytical (Malvern, UK). UV/Vis absorption spectra were measured using an UV−Vis−NIR spectrometer (Lambda 1050, from Perkin Elmer, Waltham, MA, USA). Photoluminescence (PL) spectra were detected by a FLS1000 Spectrometer from Edinburgh Instruments (Livingston, UK).

Characterization of morphology: SEM results were obtained from the field emission scanning electron microscopy (FESEM) GeminiSEM 300 (Carl Zeiss Microscopy Ltd., Jena, Germany). AFM measurements were performed by Cypher S from Oxford Instruments Asylum Research, Inc. in contact mode.

Time-of-flight secondary ion mass spectrometry: TOF-SIMS was performed using a TOF-SIMS instrument (ION TOF TOF-SIMS V), where a 10 keV Ar^+ cluster ion source was used for sputtering and a 25 keV Bi^{3+} pulsed primary ion beam was used for the analysis. The area of analysis was 150 × 150 μm^2.

Depth-profiling X-ray photoelectron spectroscopy: DP-XPS experiments performed on the Thermo Scientific XPS Escalab Xi+ using 12 kV cathode biased Al Ka radiative source. The base pressure in the analysis chamber was about 5×10^{-10} mbar. Depth profiling tests were conducted by using an Ar^+ sputtering gun operated at 1 keV with raster size of 2 mm× 2 mm.

Film-depth-dependent light absorption: Film-depth-dependent light absorption spectra were acquired by an in situ spectrometer (PU100, Shaanxi Puguang Weishi Co. Ltd.) (Shaanxi, China) equipped with a soft plasma-ion source. The power-supply for generating the soft ionic source was 100 W with an input oxygen pressure ~10 Pa. The film surface was incrementally etched by the soft ion source, without damage to the materials underneath the surface, which was in situ monitored by a spectrometer. From the evolution of the spectra and the Beer–Lambert's Law, film-depth-dependent absorption spectra were extracted. The exciton generation contour is numerically simulated upon inputting sub-layer absorption spectra into a modified optical transfer-matrix approach. The detailed experimental and numerical method are available elsewhere.[3,4]

Transient absorption measurement: The femtosecond TA experiment is carried out with a commercial transient absorption spectrometer (HELIOS, Ultrafast Systems). Ultrafast pulses at ~790 nm from a regenerative Ti:Sapphire amplifier system (Spectra Physics, Solstice) were sent into TOPAS-Prime (Light Conversion) to generate tuneable pump pulses (355 nm ~ 2600 nm). Another part was sent into a delay stage, followed by white-light generation in YAG substrate to provide broadband probe pulses (800 nm~1550 nm). The pump and probe pulses were focused onto a ~0.5 mm^2 spot. The time resolution of the laser pulses is estimated around 120 fs. The samples were measured in a chamber with the steady flow of nitrogen gas. Nanosecond TA experiments were based on an Astrella Ti:Sapphire amplifier (Coherent; 800 nm, 35 fs, 7 mJ pulse^{-1} and 1 kHz repetition rate). Briefly, the pump pulse was generated by a TOPAS Optical Parametric Amplifier (OPA) at 532 nm with pulse duration of 0.8 ns. The white light continuum (WLC) probe beam was generated by focusing a Nd:YAG laser into a photonic crystal fiber and the pump-probe delay was controlled by a digital delay generator (CNT-90, Pendulum Instruments).

Grazing-incidence wide-angle X-ray scattering: GIWAXS in Figure S9 were performed at the Synchrotron & Printable Electronic Lab, Hoffmann Institute of Advanced Materials, Shenzhen Polytechnic with SAXS Focus 3.0 equipped with a Cu X-ray Source (8.05 keV, 1.54 Å) and a EIGER 2R 500K detector. The incidence angle is 0.2° and the distance of sample to detector is 75 mm. GIWAXS in Figure S22 was measured at 13A beam line of National Synchrotron Radiation Research Center (NSRRC, Taiwan). All samples for GIWAXS were radiated at 12 keV X-ray with an incident angle of 0.2°.

Calculation of the vertical distribution via D-XPS

The weight percentage of PM6 in PM6:BTP-eC9 film can be described as follows:

$$PM6\% = \frac{m_{PM6}}{m_{PM6} + m_{eC9}} = \frac{n_{PM6}M_{PM6}}{n_{PM6}M_{PM6} + n_{eC9}M_{eC9}} \qquad (2)$$

$$PM6\% = \frac{1}{1 + \frac{n_{eC9}M_{eC9}}{n_{PM6}M_{PM6}}} \qquad (3)$$

The ratio of O/Cl can be expressed as:

$$\frac{O}{Cl} = \frac{2n_{PM6} + 2n_{eC9}}{2n_{eC9}} \qquad (4)$$

nPM6 and neC9 are the mole number of PM6 and BTP-eC9, respectively. M_{PM6} and M_{eC9} are the molecular weight of a single unit of PM6 and BTP-eC9, which are 1218 and 1572, respectively. Therefore, we can deduce the PM6 weight contents from equations (2)-(4) as follows:

$$PM6\% = \frac{1}{1 + \frac{1.29}{2\frac{O}{Cl} - 1}} \qquad (5)$$

The atom ratio O/Cl was calculated by the integration of areas of corresponding XPS peaks and the atomic sensitivity factors. The simplified equation is O/Cl atom ratio = (O peak area/O sensitivity factor)/(Cl peak area/Cl sensitivity factor). Empirically derived set of atomic sensitivity factors for XPS can be acquired at http://202.38.64.11/~mams/escalab/sfactors.html.

Certification report of PM6:BTP-eC9 solar cells

170209260120

中国认可
国际互认
检测
TESTING
CNAS L0921

第 1 页 *page* 1
共 4 页 *This report includes* 4 *page*

天津市计量监督检测科学研究院
电子仪表实验所

TIANJIN INSTITUTE OF METROLOGICAL SUPERVISION AND TESTING
ELECTRONIC & INSTRUMENTAL LABORATORY

检测报告
TEST REPORT

报告编号： TDYF 字第 230071-WT 号
Report №

产品名称： 太阳电池
Name Solar cells

规格型号： PM6:BTP-eC9
Model

委托单位： 深圳技术大学 新材料与新能源学院
Applicant Shenzhen Technology University, College of New Materials and New Energy

生产单位： 深圳技术大学 新材料与新能源学院
Manufacturer Shenzhen Technology University, College of New Materials and New Energy

检验检测专用章
stamp

地址 Add：天津市河西区五号堤路 18 号 №. 18 WuHaoDi Road Hexi District Tianjin
电话 Tel：022-81264268 传真 Fax：022-28326590 电邮 Email：tjpvtc@163.com
网址 Web：http://www.tjelab.com

资质认定合格证书号：170209260120

Certificate № of CMA：170209260120

中国合格评定国家认可委员会认可证书：**№.CNAS L0921** 号

Certificate approved by CNAS：№.CNAS L0921 号

说明：

⑴根据与 CNAS 相关协议，同意使用 ILAC-MRA/CNAS 国际互认联合标识。

⑵本报告封面和骑缝位置无“天津市计量监督检测科学研究院电子仪表实验所检验检测专用章”无效。

⑶复制报告封面和骑缝位置未重新加盖“天津市计量监督检测科学研究院电子仪表实验所检验检测专用章”无效。

⑷本报告无主检、审核、批准人员签字无效。

⑸本报告涂改无效。

⑹非经本所抽样，本报告仅对送检样品负责。

Statement

⑴According to the agreement of CNAS, agree to use the logo of ILAC-MRA/CNAS.

⑵This report will be invalid without 'special seal for test' on the cover and the perforation.

⑶The report copy is invalid if it is not affixed the 'special seal for test' on the cover and the perforation.

⑷This report will be invalid without the signatures of the inspector, examiner and approver.

⑸This report will be invalid if altered.

⑹If the samples aren't sampled by us, this report is only responsible for those samples which are sent to us for testing.

天津市计量监督检测科学研究院电子仪表实验所
Tianjin Institute of Metrological Supervision and Testing Electronic & Instrumental Laboratory

检测报告
TEST REPORT

№：TDYF 字第 230071-WT　　　　共 4 页 第 2 页

委托单位 Applicant	深圳技术大学新材料与新能源学院 Shenzhen Technology University, College of New Materials and New Energy	单位地址 Address	广东省深圳市坪山区深圳技术大学 B2 新材料与新能源学院 Shenzhen Technology University B2, College of New Materials and New Energy, Shenzhen,Guangdong	
产品名称 Name	太阳电池 Solar cells	商　标 Trademark	—	
规格型号 Model	PM6:BTP-eC9	生产日期 Date	—	
产品编号 Number	SZTU-PM6-03	检测类别 Sort	委托检测 Request examination	
检测依据 Reference documents for the test	IEC 60904-1:2020《光伏器件 第 1 部分：光伏电流-电压特性的测量》 Photovoltaic devices – Part 1: Measurement of photovoltaic current-voltage characteristics			
样　品 Sample	样品来源 Source	送样 Sample delivery	样品状态 Condition	外观良好 Normal
	样品数量 Quantity	1 片	收样日期 Date of receiving	2023 年 Year 11 月 Month 30 日 Day
检测地点 Place	天津市河西区五号堤路 18 号 106 室 Room 106,No.18 WuHao Di Road,Hexi Distric,Tianjn			
环境条件 Environment	温度 Temperature 25°C	相对湿度 Relative humidity 40％	气压 Pressure —	
检测自 Test begin from	2023 年 Year 11 月 Month 30 日 Day	至 To	2023 年 Year 11 月 Month 30 日 Day	
主　检 Inspector	周超　杨雪辰			
审　核 Examiner	冯宇			
批　准 Approver	杨学毫　杨学亮			
			签发日期：2023 年 Year 11 月 Month 30 日 Day Date of issue	
备注： Remarks	—			

检测用主要仪器设备一览表
Equipments for Test

序号 №	仪器设备名称 Name	规格型号 Model	设备编号 Serial №	证书有效期 Valid date of verification	备注 Remarks
1	电池片 I-V 特性测试仪 I-V Tester for Solar Cells	VS-6831S	21VJ002	2024. 09. 10	—
2	红外测温仪 Infrared thermometers	562	51350514WS	2024. 03. 12	—
3	Keithley 2400 Standard Series Sourcemeter	2400	4463530	2024. 08. 31	—

样品信息
Information for Samples

样品编号 Sample Number	规格型号 Sample Type	产品编号 Serial Number
230071-1	PM6:BTP-eC9	SZTU-PM6-03

检测报告
TEST REPORT

№：TDYF 字第 230071-WT

检测内容： Test content	光伏电流-电压特性 *I-V* Characteristic		
序号 №	项目 Item	技术要求 Requirement	检测结果 Test result
1	光伏电流-电压特性 *I-V* Characteristic	—	见下表 As follows

测试时间 Date	2023. 11. 30
测试条件 Condition	使用稳态 AAA 级太阳模拟器，在 AM1. 5G，1000W/m²，25. 0℃条件下测试 Sample was tested under the condition of AM1.5G, 1000W/m², 25.0°C with a steady-state class calibrated AAA solar simulator
有效面积 Active area	0. 0425cm² 备注：器件的有效面积是由带固定孔径的薄金属掩膜板量化 Remark: Designated area defined by thin metal aperture mask.

样品编号 №	V_{oc} (V)	I_{sc} (mA)	J_{sc} (mA/cm²)	P_{max} (mW)	V_{Pmax} (V)	I_{Pmax} (mA)	FF (%)	η (%)
230071-1	0. 841	1. 183	27. 84	0. 787	0. 680	1. 158	79. 10	18. 52

测试程序 Test program settings	起始电压： Starting voltage:	+1. 00V
	终止电压： Termination voltage:	-0. 20V
	扫描间隔： Scan interval:	0. 02V
	延迟时间： Delay time:	0. 1s

I-V 曲线图
I-V curve

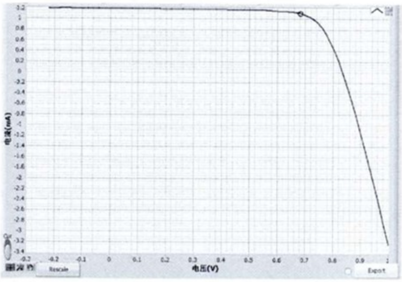

本报告结束 **The end of the report**

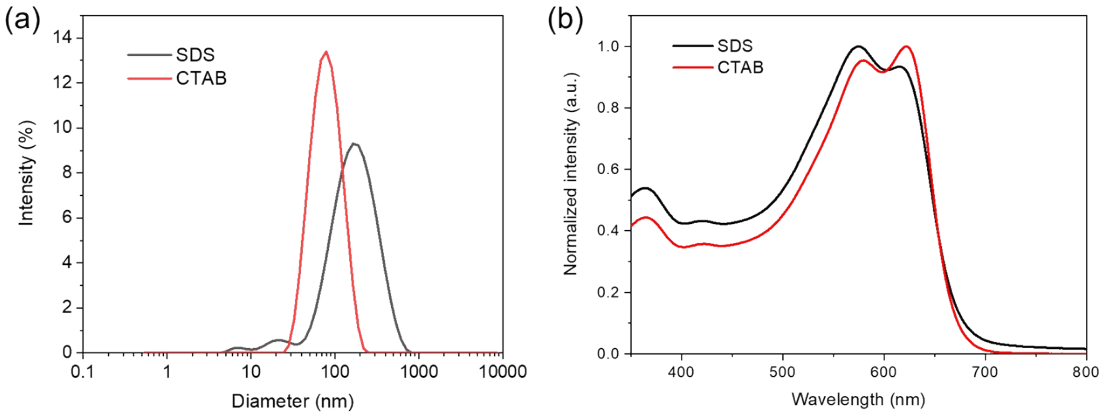

Figure S1. (a) Particle size distribution and (b) UV–vis absorption spectra of SDS and CTAB-prepared PM6 NP inks.

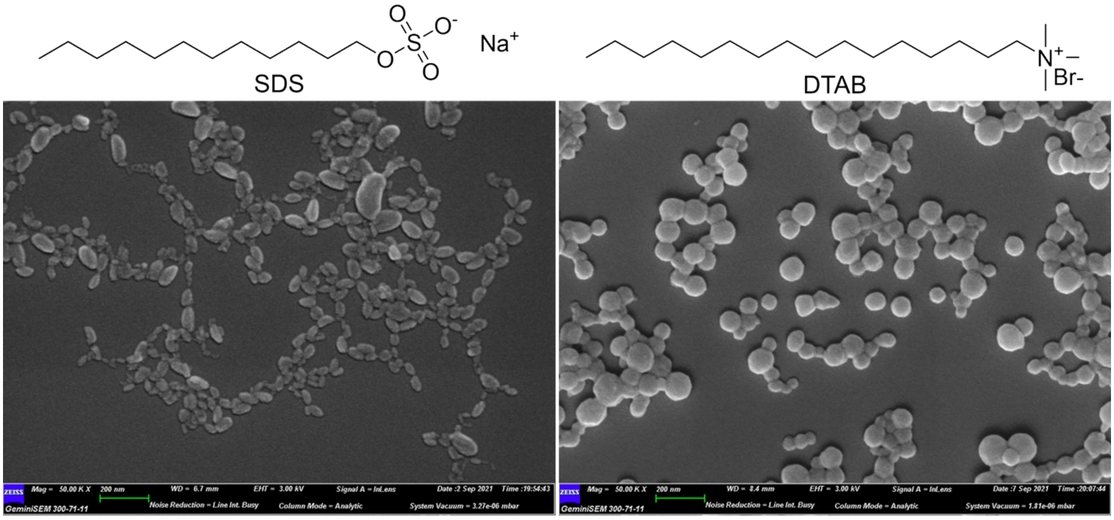

Figure S2. SEM of dilute SDS and CTAB-prepared PM6 NP inks processed on silicon slides.

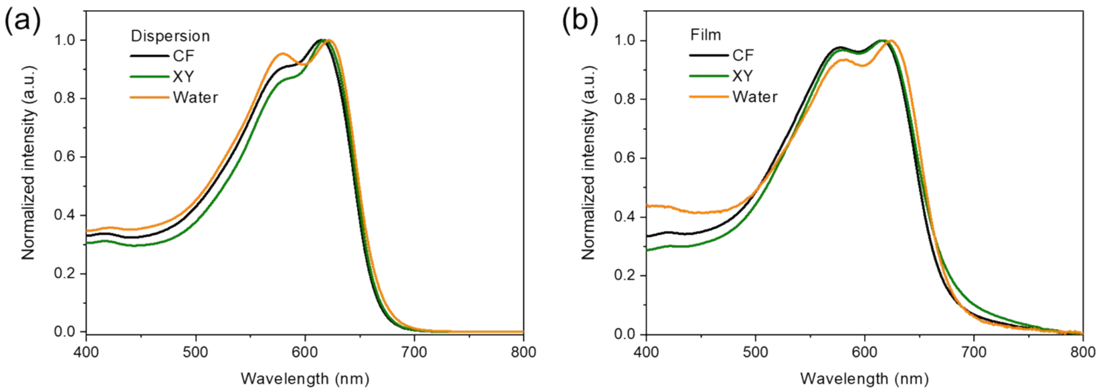

Figure S3. UV–vis absorption spectra of PM6 (a) solutions and (b) films processed by different solvents.

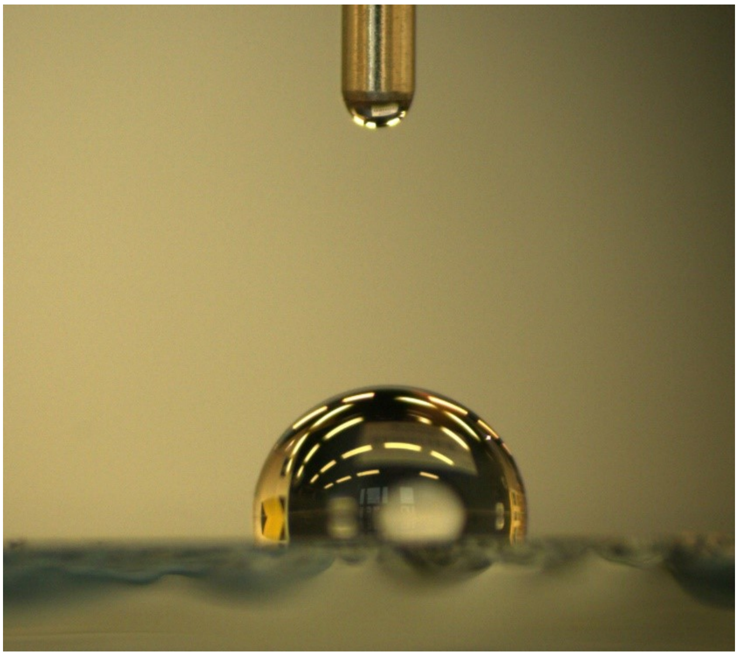

Figure S4. Contact angle image of water on top of mesostructured PM6 film.

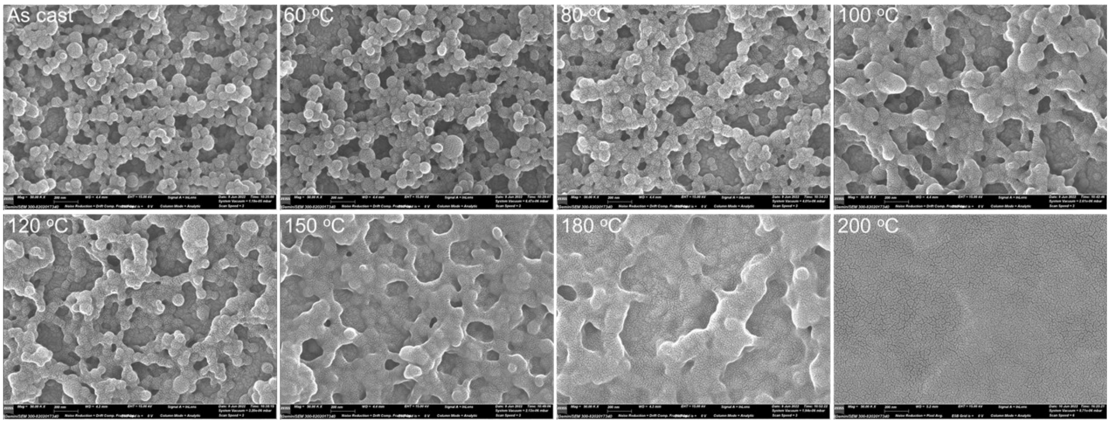

Figure S5. SEM of PM6 mn-films after different thermal annealing.

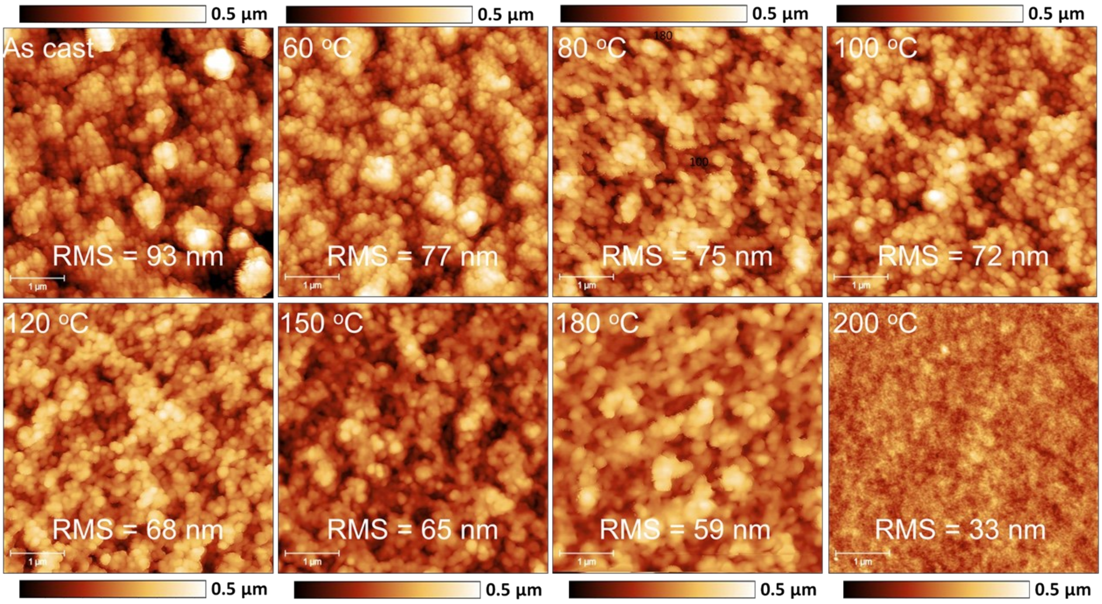

Figure S6. AFM of PM6 mn-films after different thermal annealing.

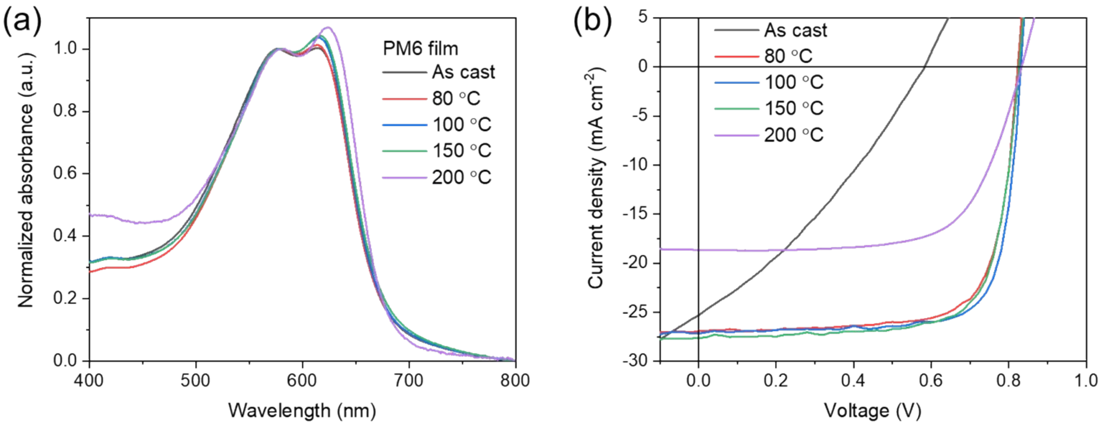

Figure S7. (a) UV–vis absorption spectra of PM6 film and (b) mn-LBL-processed solar cells under different thermal annealing.

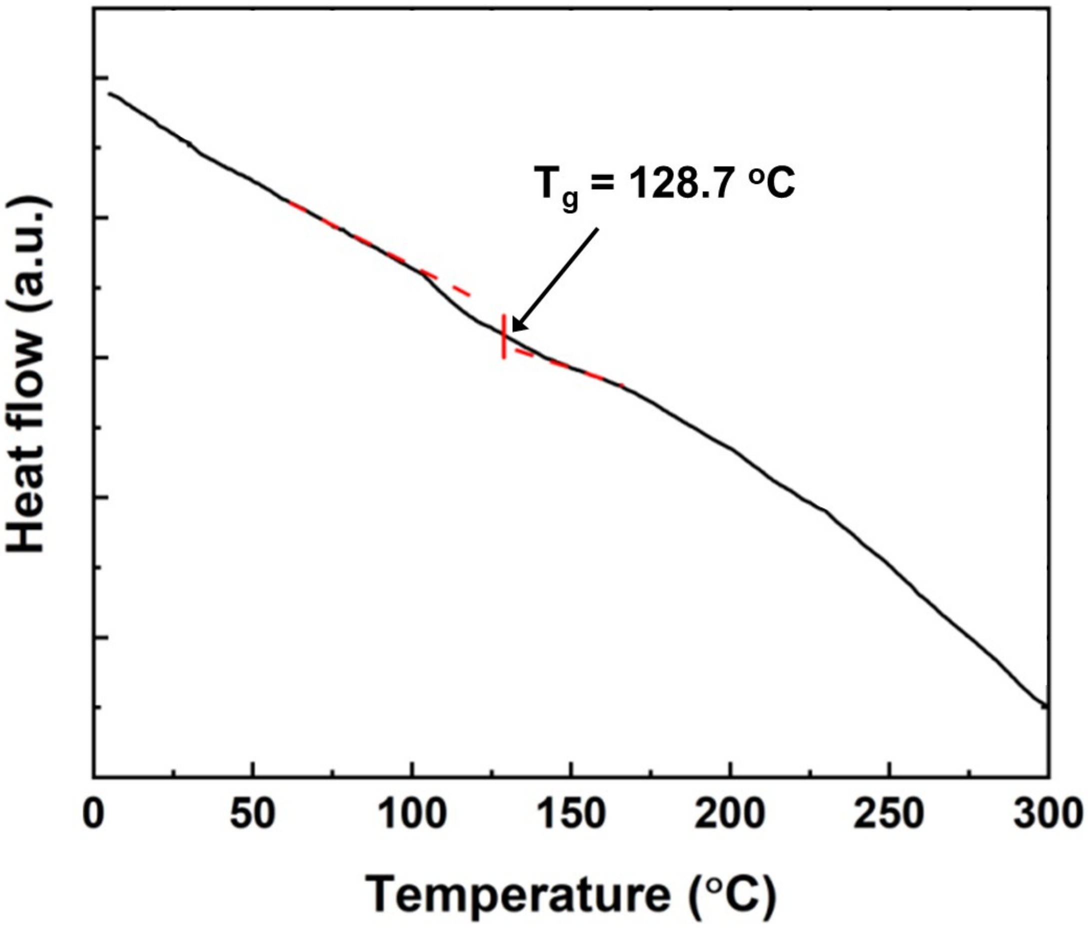

Figure S8. DSC scan of PM6.

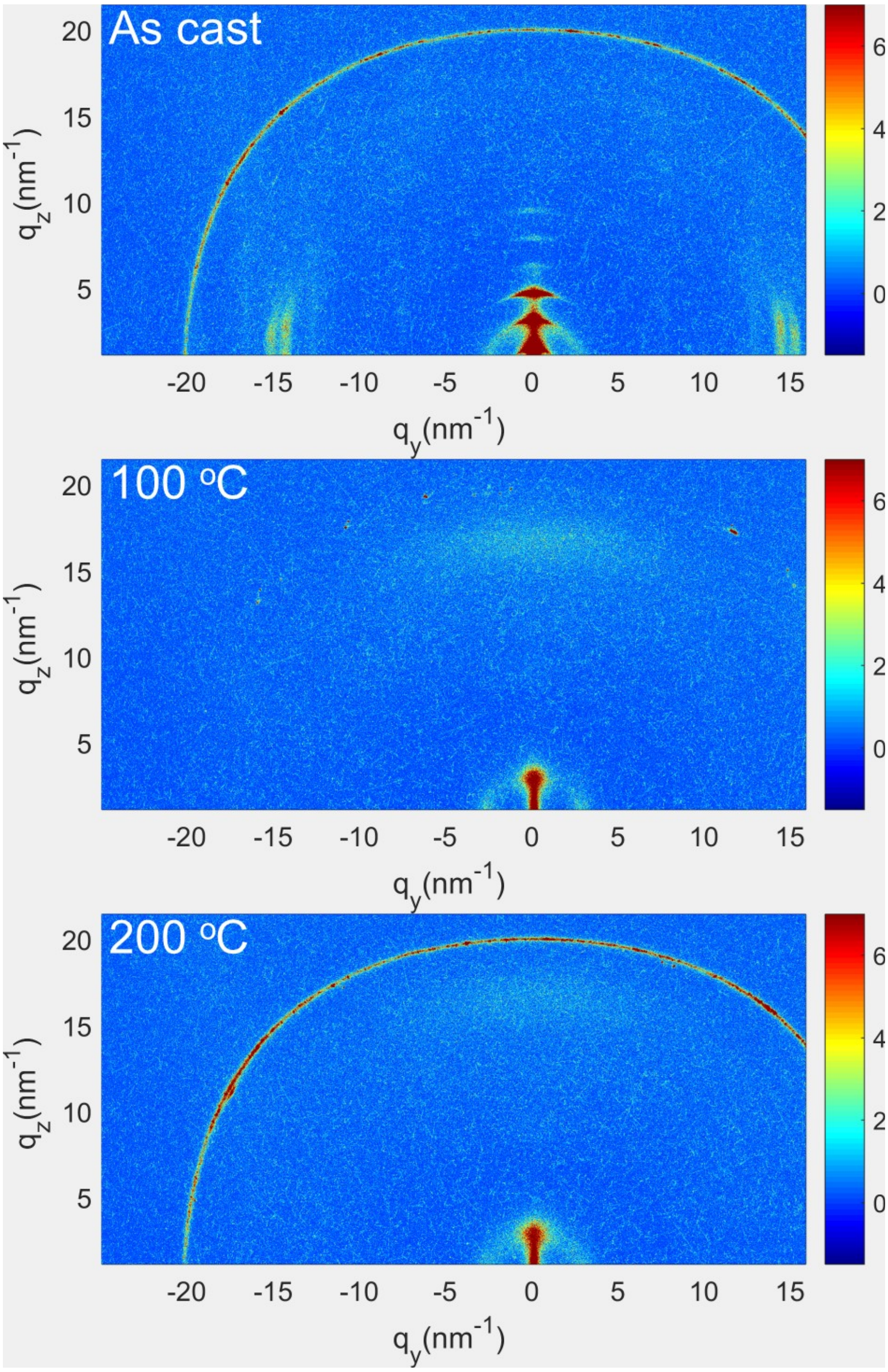

Figure S9. 2D GIWAXS patterns of PM6 mn-films after different thermal annealing.

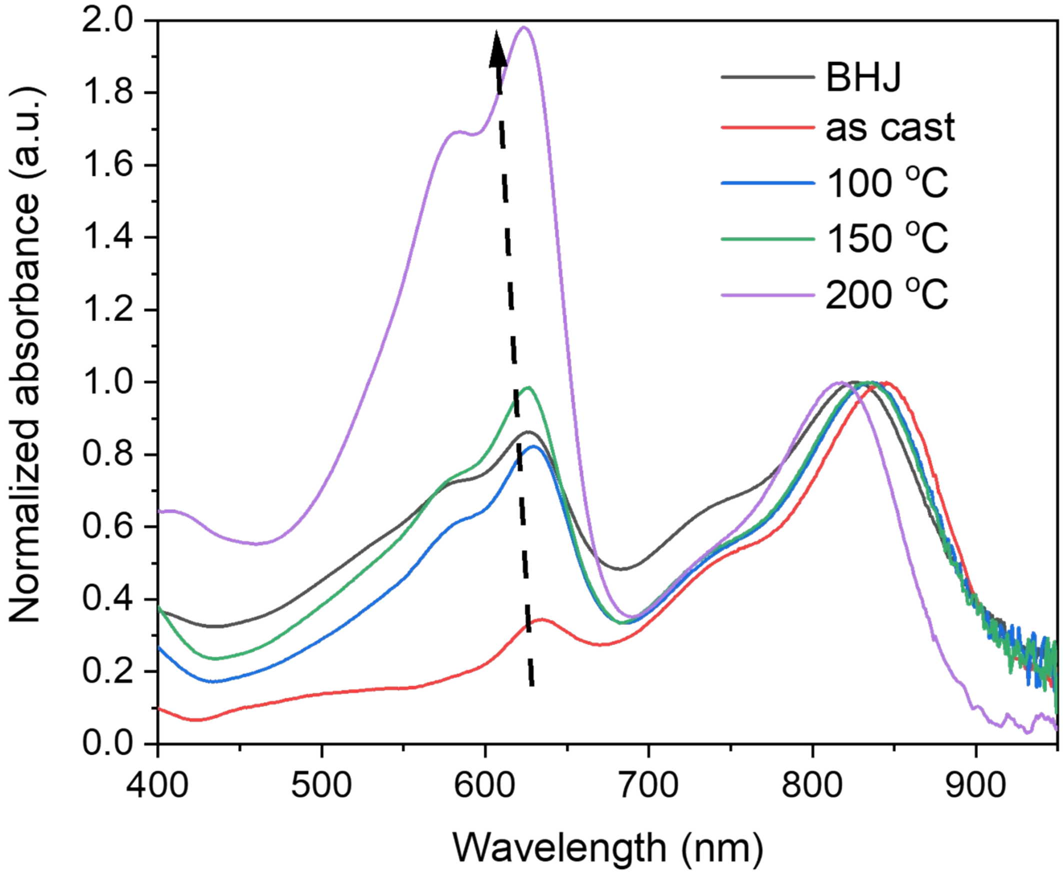

Figure S10. UV-vis absorption spectra of PM6:BTP-eC9 mn-LBL films with mn-layers under different thermal annealing.

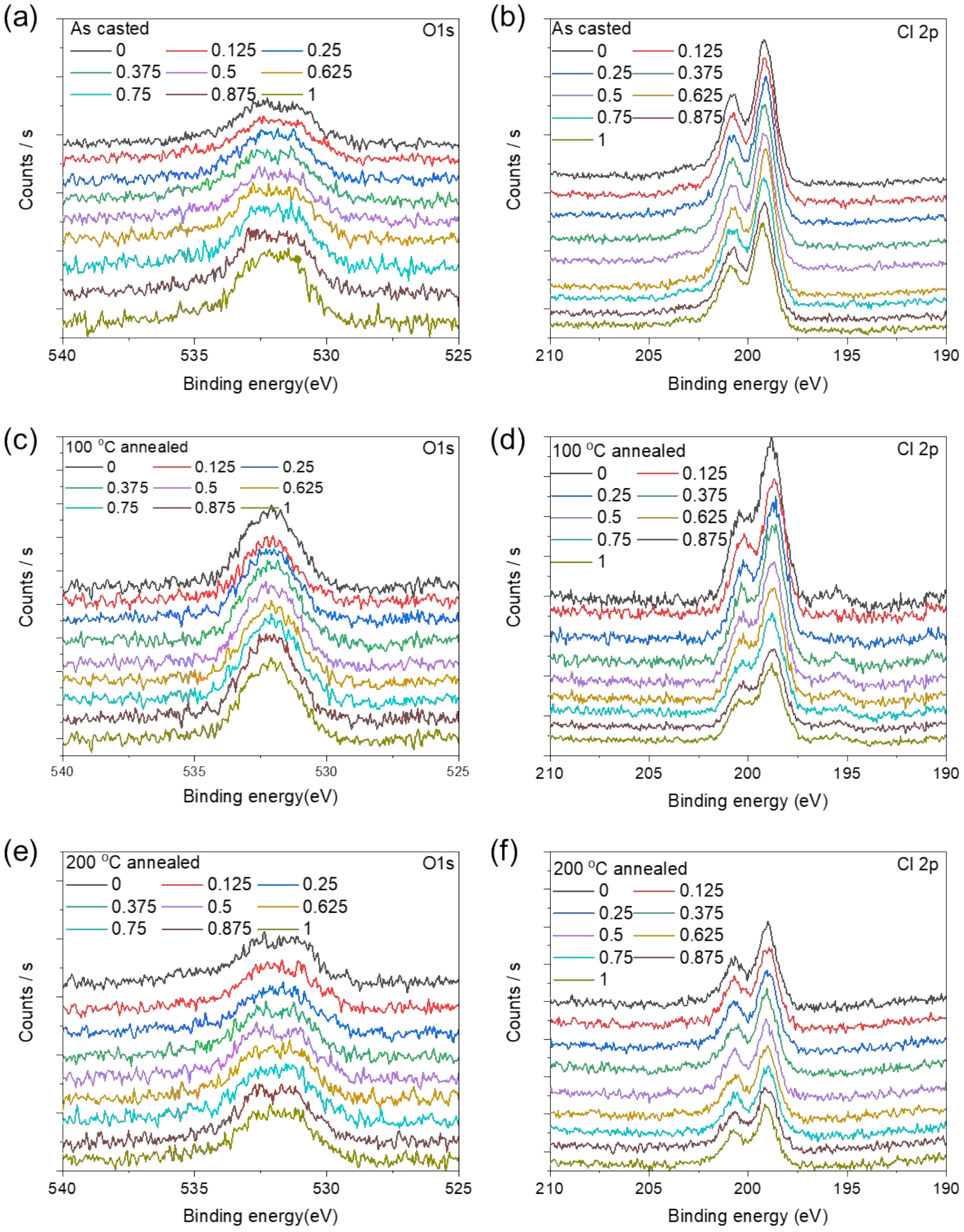

Figure S11. Figure S. XPS scans as a function of normalized depth of mn-LBL films with (a,b) as casted, (c,d) 100 ºC annealed and (e,f) 200 ºC annealed PM6 layer in the (a,c,e) O1s and (b,d,f) Cl2p binding regions.

Table S1. Photovoltaic parameters of PM6:BTP-eC9 devices with mn-donor layer under different thermal treatments.

Annealing temperature	Voc (V)	Jsc (mA cm^{-2})	FF (%)	PCE (%)
As cast	0.581	25.05	31.59	4.60
80 °C	0.822	26.93	74.89	16.58
100 °C	0.828	27.17	76.88	17.30
150 °C	0.825	27.62	74.14	16.89
200 °C	0.833	18.65	67.14	10.43

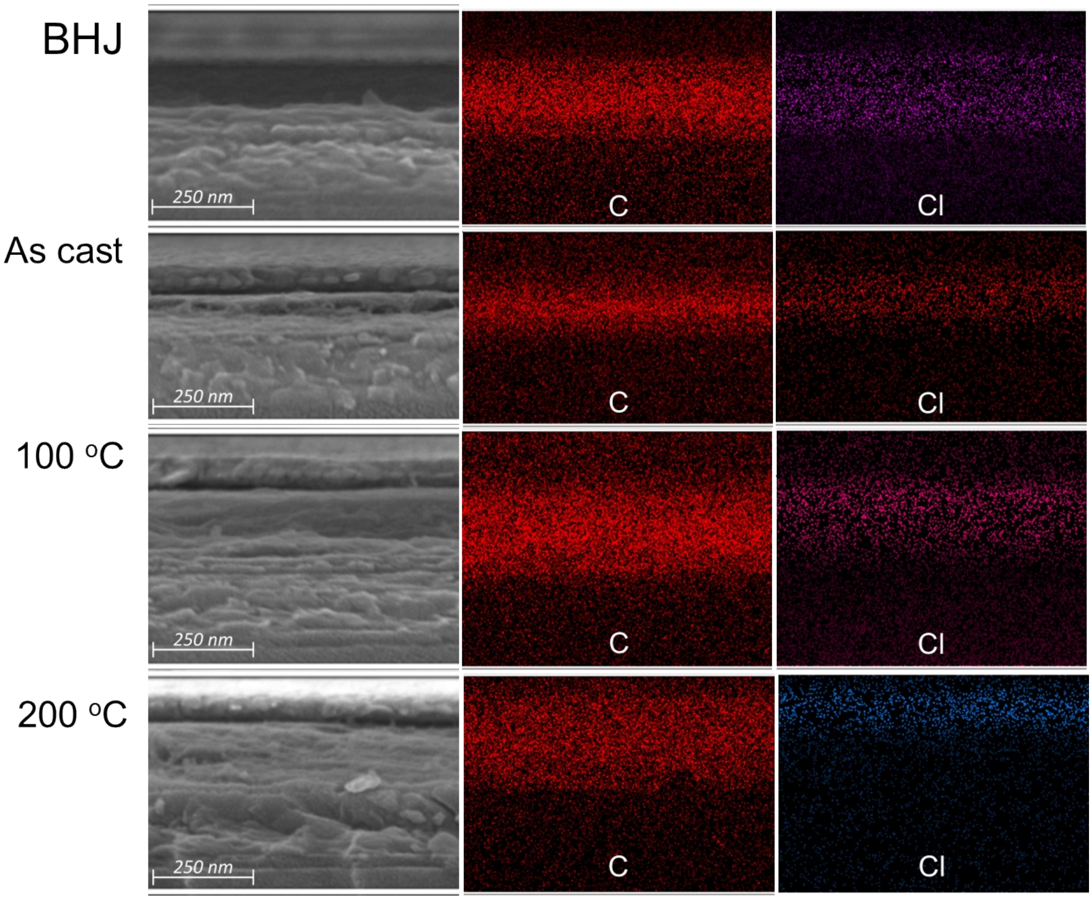

Figure S12. Cross-sectional SEM of PM6:BTP-eC9 mn-LBL films with mn-layers under different thermal annealing.

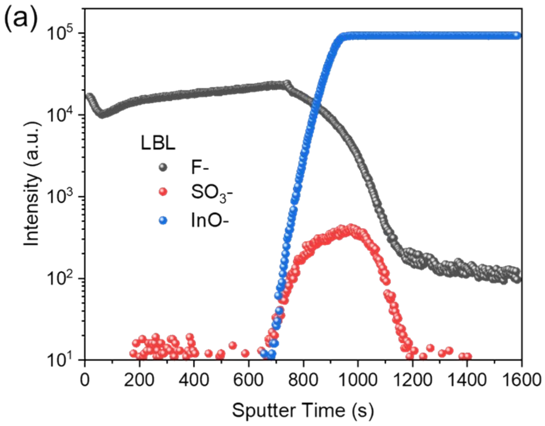

Figure S13. TOF-SIMS ion of (a) c-LBL and (b) mn-LBL films processed by XY solution.

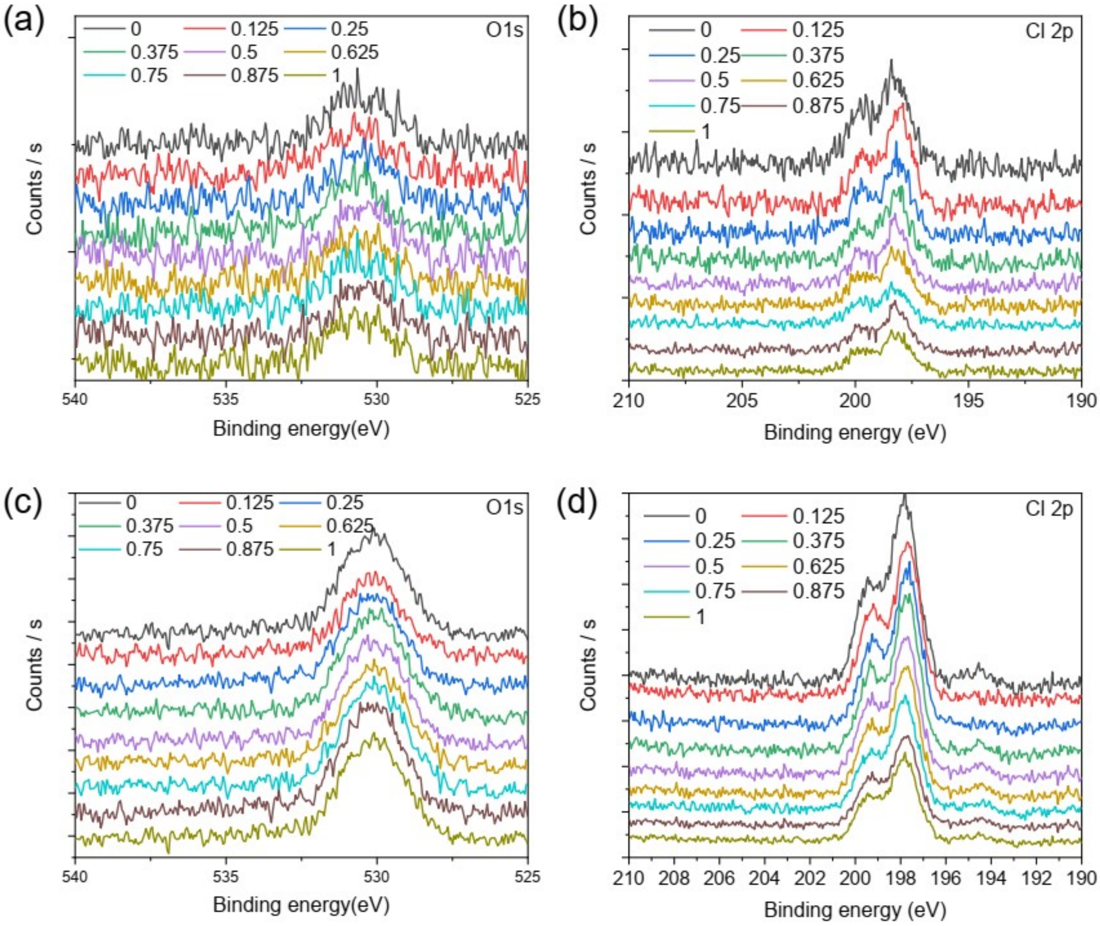

Figure S14. XPS scans as a function of normalized depth of 250 nm-thick PM6:BTP-eC9 films processed by (a,b) conventional LBL and (c,d) BHJ techniques in the (a,c) O1s and (b,d) Cl2p binding regions.

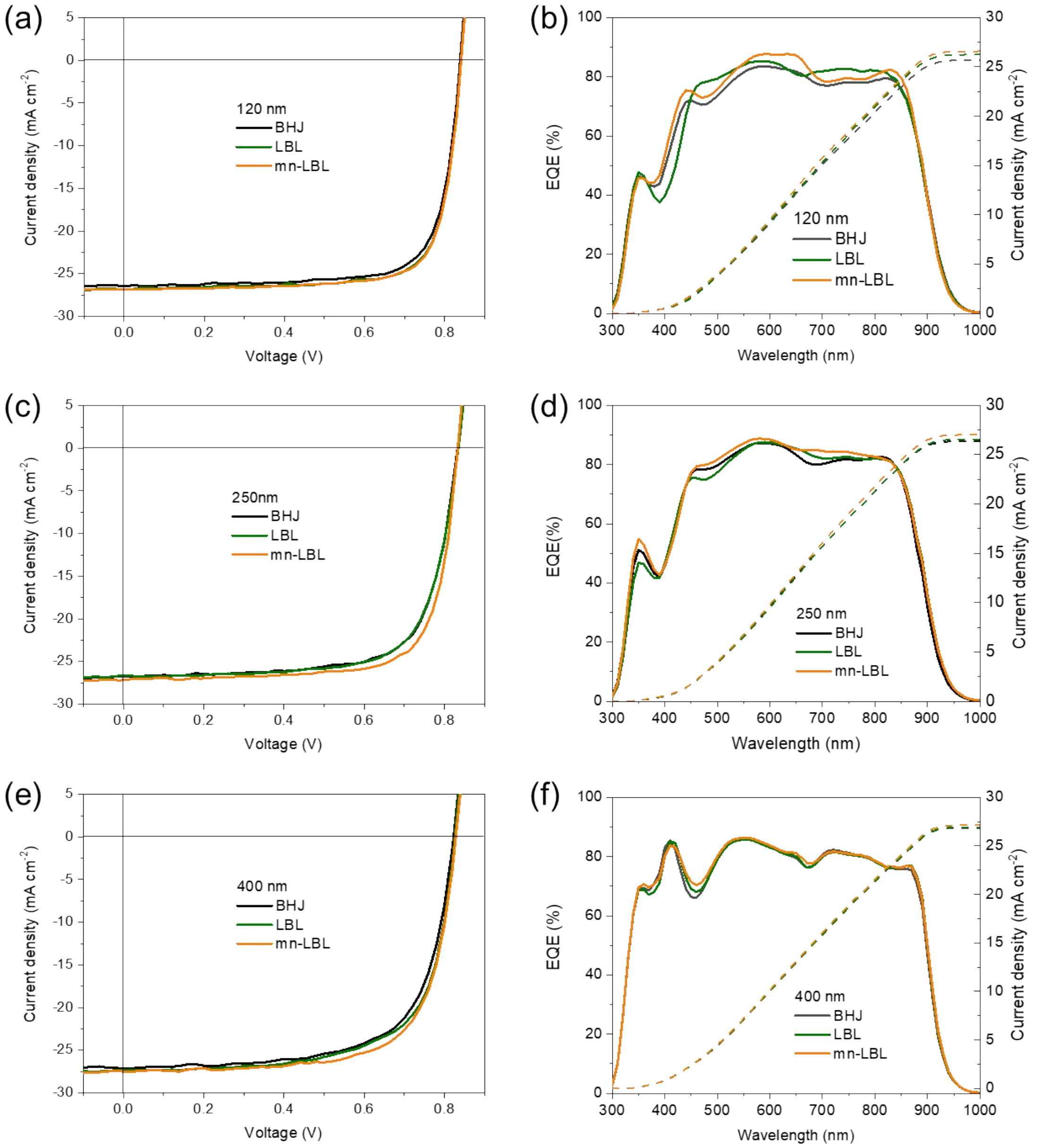

Figure S15. (a,c,e) J-V curves and (b,d,f) EQE spectra of PM6:BTP-eC9 devices prepared by BHJ, conventional LBL and mn-LBL techniques with active layer thickness of (a,b) 120 nm, (c,d) 250nm and (e,f) 400 nm.

It is shown that thickened devices exhibit higher EQE around 400-600 nm. As is known, most of the incident light is absorbed near the transparent electrode side (the substrate), that means most of the excitons are generating and disassociating near this region, which can be confirmed from the FLAS results. Thus, in the LBL device with high thickness, the lower proportion of acceptor near the substrate region would restrict the electron transport and collection.[5] In addition, **Figure S39** shows that the relatively higher PM6 fraction on the bottom and less PM6 on top of 400 nm active layer, indicating more pronounced EQE around the donor regime.

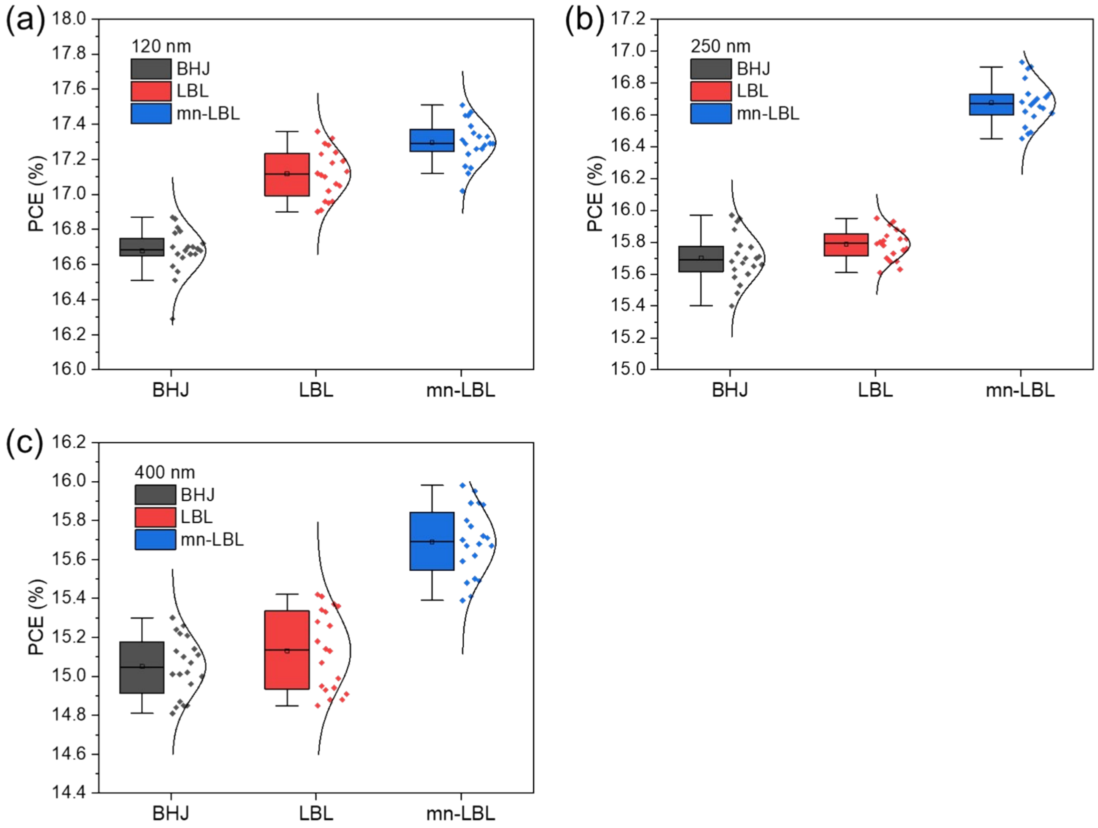

Figure S16. Comparison of PCEs of PM6:BTP-eC9-based OSCs prepared by BHJ, c-LBL and mn-LBL process as box plots (sample minimum, 25th percentile, median, 75th percentile and maximum) from 20 devices.

Table S2. Classification of representative OSCs with thick active layer.

NO.	Year	Active layer	Thickness (nm)	PCE (%)	URL
1	2017	PFBT4T-C5Si-25%:PC$_{71}$BM	270	10.39	https://doi.org/10.1039/C7TA05583H
			380	10.95	
			420	11.09	
2	2017	PTB7-Th:BTR:PC$_{71}$BM	200	10.19	https://doi.org/10.1021/jacs.6b11991
			230	10.34	
			250	10.37	
			275	9.99	
			300	9.83	
			400	8.37	
3	2017	PBDBTF:IDTN	205	11.3	https://doi.org/10.1002/adma.201704051
			270	10.8	
			300	10.1	
			380	9.4	
			530	8.5	
4	2018	PM6:IT4F	200	12.8	https://doi.org/10.1007/s114

			285	12.2	26-017-9199-1
			330	11.7	
5	2018	PM6:SeTIC4Cl	200	11.8	https://doi.org/10.1021/acsenergylett.8b01808
			250	11.5	
			300	11.3	
6	2018	PTQ10: IDIC	210	11.59	https://doi.org/10.1038/s41467-018-03207-x
			230	10.97	
			270	10.43	
			310	10.31	
7	2018	PTQ10: IDTPC	200	11.7	https://doi.org/10.1002/aenm.201800856
			260	11	
			315	10.6	
			400	10	
			505	9.2	
8	2018	BTR:NITI:PC$_{71}$BM	300	13.63	https://doi.org/10.1038/s41560-018-0234-9
9	2019	PM6:Y6	200	14.3	https://doi.org/10.1016/j.joule.2019.01.004
			250	14.1	
			300	13.6	
10	2019	PBTA-Si:PTzBI-Si:N220	380	10.4	https://doi.org/10.1038/s41467-019-12132-6
11	2019	BTR-Cl:Y6	200	10.04	https://doi.org/10.1016/j.joule.2019.09.009
			300	9.57	
			400	9	
12	2019	PM6:F-2Cl	200	11.93	https://doi.org/10.1002/aenm.201902688
			250	10.51	
			350	9.03	
13	2020	Si25-H2:IEICO-4F	210	11.58	https://doi.org/10.1039/d0ta01340d
			250	12.02	
			320	13.2	
			380	12.79	
14	2020	PT2:TTPTTT-4F:IDIC	200	11.8	https://doi.org/10.1002/solr.202000476
			300	12.1	
			400	12.2	
15	2020	PBDB-T-2Cl:BP-4F:PC$_{61}$BM	200	15.3	https://doi.org/10.1007/s11426-019-9556-7
			300	14.3	
16	2020	D18:Y6:PC$_{61}$BM	200	16.63	https://doi.org/10.1016/j.scib.2020.08.027
			270	16.51	
			300	16.32	
			350	16.19	
17	2020	PBDB-TF:BTP-4Cl	328	15	https://doi.org/10.1021/acsami.0c05172
			545	13.8	
			1020	12.1	

18	2020	PM7:MF1	200	12.37	https://doi.org/10.1002/adfm.201908336
			255	12.27	
			312	12.03	
			378	11.6	
		PM7:MF2	197	13.39	
			251	12.89	
			308	12.34	
			373	11.58	
19	2020	PBDB-T-2Cl:BP-4F:MF1	200	15.04	https://doi.org/10.1039/C9EE04020J
			300	14.7	
			380	13.38	
20	2020	PM6:Y6:BTP-M	200	15.15	https://doi.org/10.1039/C9EE03710A
			300	14.23	
			400	13.48	
21	2020	PBT(E)BTz :PBDB-TF:BTP-4Cl	200	15.21	https://doi.org/10.1002/adfm.201910466
			250	14.61	
			300	14	
22	2020	P2FEhp:Y6	210	11.4	https://doi.org/10.1007/s10118-020-2355206-3
			520	10.5	
23	2021	PM6:BTP-eC9	300	16.25	https://doi.org/10.1038/s41467-017.4821-25148-8
			400	15.12	
			500	14.37	
24	2021	PM6:FCC-Cl	200	12.3	https://doi.org/10.1016/j.joule.2021.03.020
			300	10.9	
			400	9.0	
25	2021	PM6: BP4T-4F: BP3T-4F	200	16.89	https://doi.org/10.1002/solr.202100365
			250	16.58	
			300	16.03	
26	2022	PM6:BTP-4F-12:IT-M	200	17.08	https://doi.org/10.1016/j.cej.2021.129276
			250	15.89	
			300	15.34	
27	2022	PM6:Y7-BO:Y6-1O	200	17.57	https://doi.org/10.1002/adfm.202200807
			250	17.10	
			300	16.61	
			360	16.23	
			400	15.71	
28	2022	PM6:BTP-eC9	300	15.62	https://doi.org/10.1038/s41467-022-29803-6
			500	13.14	
		PM6:BTP-eC9:L8-BO-F	300	17.31	
			500	15.21	
29	2023	PM6:L8-BO	300	16.56	https://doi.org/10.1002/adma.202304225
			400	15.61	
			500	14.33	

		PM6:L8-BO:DY-TF	300	18.23	
			400	17.25	
			500	15.91	
30	2023	PM6:BTP-eC9	250	16.93	This work
			400	15.98	
		PM6:BTP-eC9 (DTT)	250	18.19	
			400	17.22	

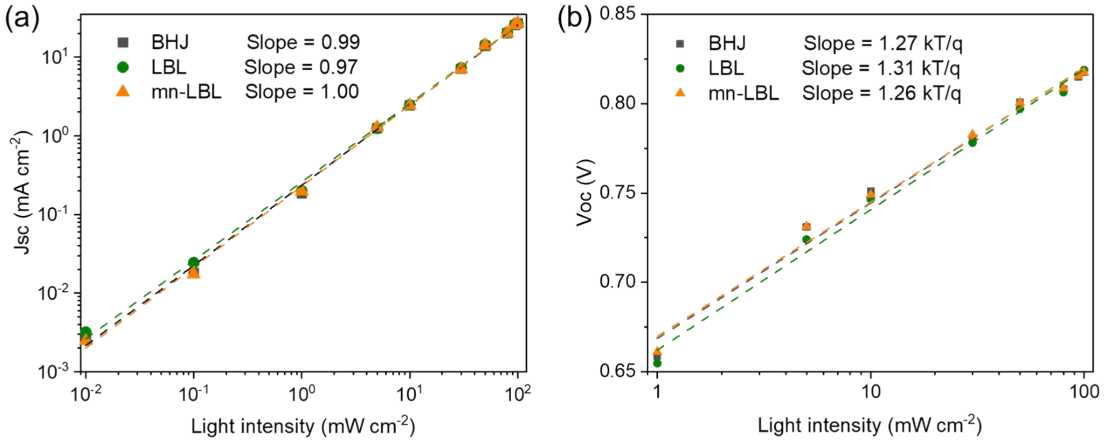

Figure S17. (a) J_{SC} and (b) V_{OC} as a function of light intensity of PM6:BTP-eC9 devices prepared by BHJ, conventional LBL and mn-LBL techniques with active layer thickness of 250 nm.

Table S3. Hole mobility and electron mobility of PM6:BTP-eC9 based OSCs prepared by BHJ, c-LBL and mn-LBL technique with a thickness of 250 nm.

Active layer	Hole mobility (× 10^{-4} cm^2 V^{-1} s^{-1})	Electron mobility (× 10^{-4} cm^2 V^{-1} s^{-1})	μ_h/μ_e
BHJ	7.13	2.15	3.32
LBL	7.19	5.16	1.39
mn-LBL	8.06	6.15	1.31

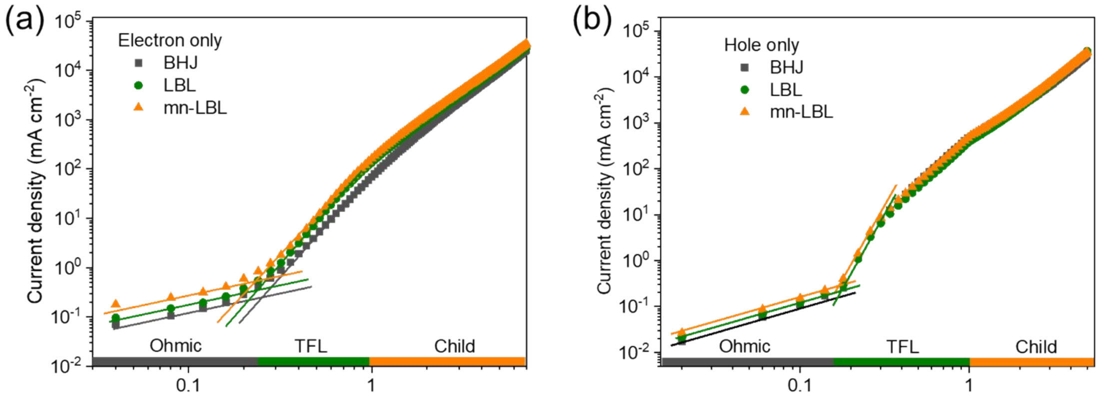

Figure S18. Dark current curves of (a) electron only and (b) hole only PM6:BTP-eC9 devices prepared by BHJ, conventional LBL and mn-LBL techniques with active layer thickness of 250 nm.

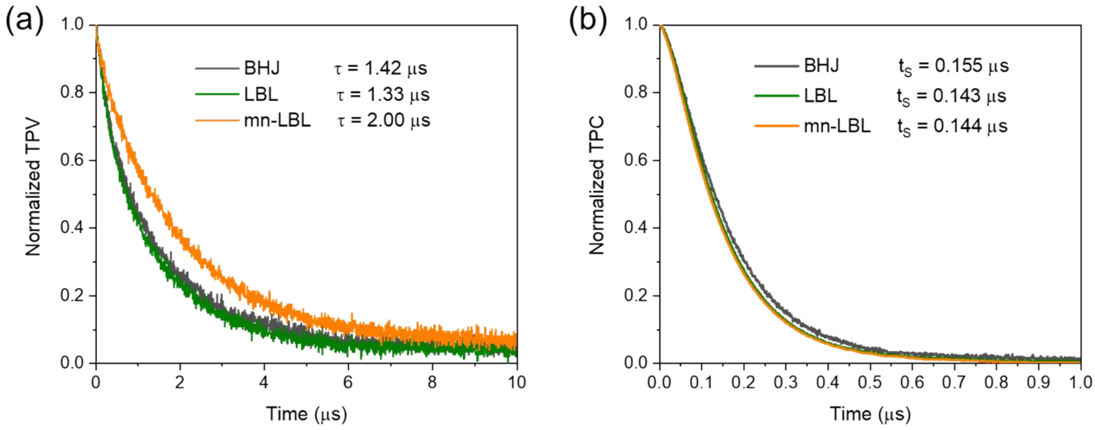

Figure S19. Normalized (a) TPV and (b) TPC curves of PM6:BTP-eC9 devices prepared by BHJ, conventional LBL and mn-LBL techniques with active layer thickness of 250 nm.

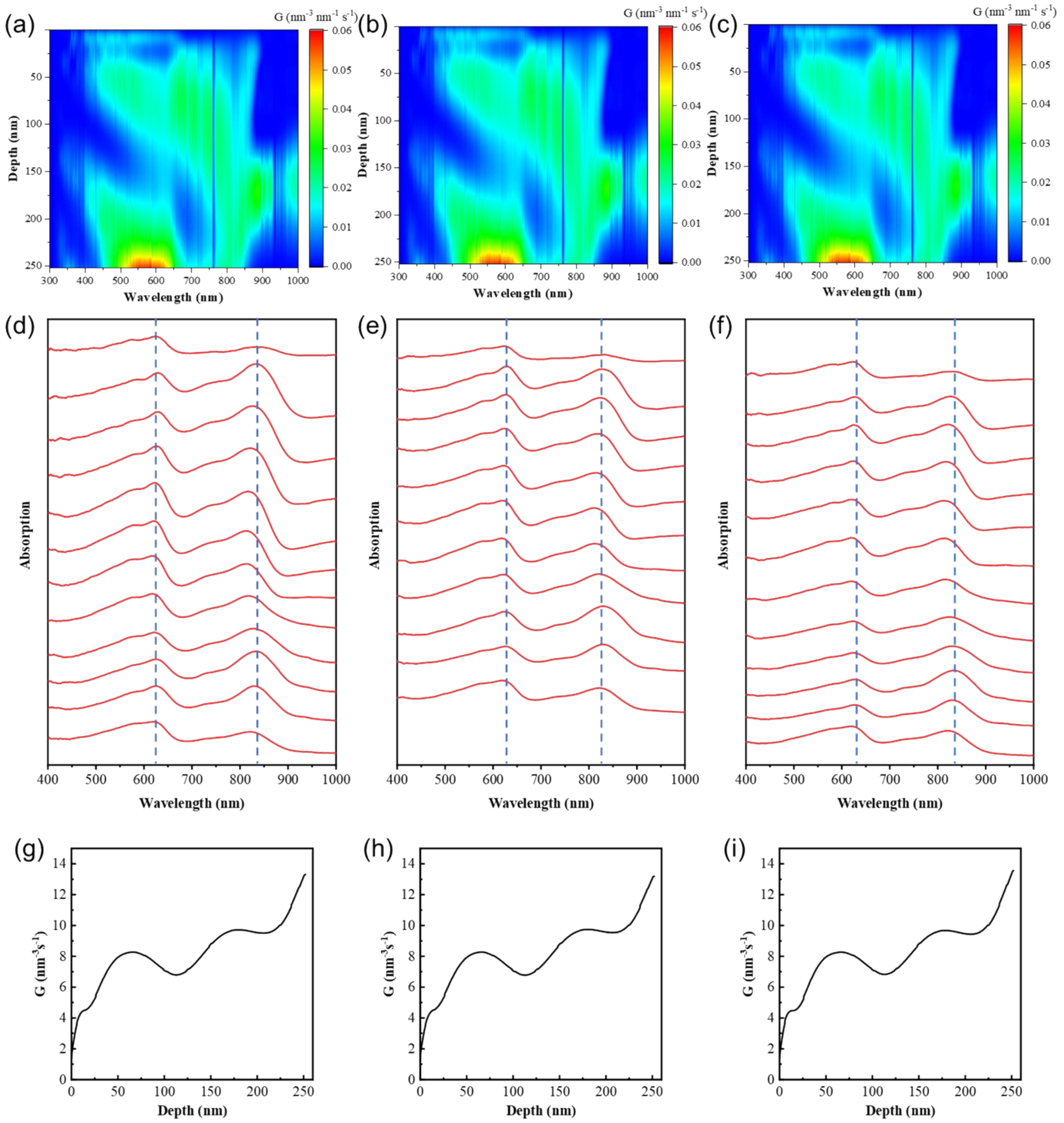

Figure S20. (a,b,c) Exciton generation contours (d,e,f) FLAS and (g,h,i) exciton generation profile of (a,d,g) BHJ, (b,e,h) conventional LBL and (c,f,i) mn-LBL processed PM6:BTP-eC9 films.

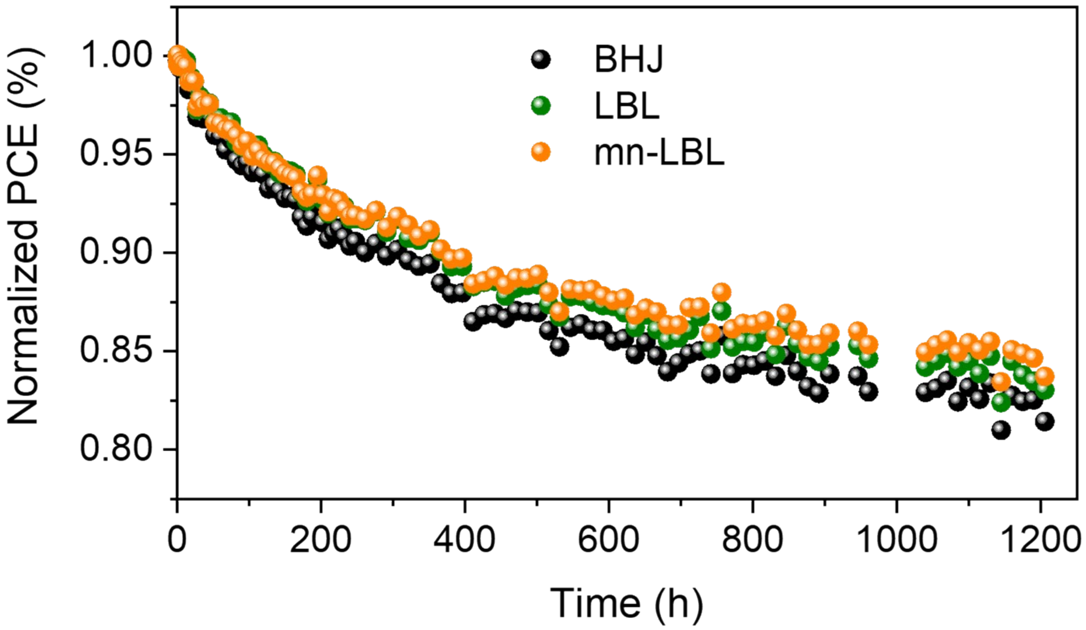

Figure S21. Photostability of PM6:BTP-eC9 devices prepared by BHJ, conventional LBL and mn-LBL techniques with active layer thickness of 250 nm under continuous 1 sun illumination in N_2 atmosphere.

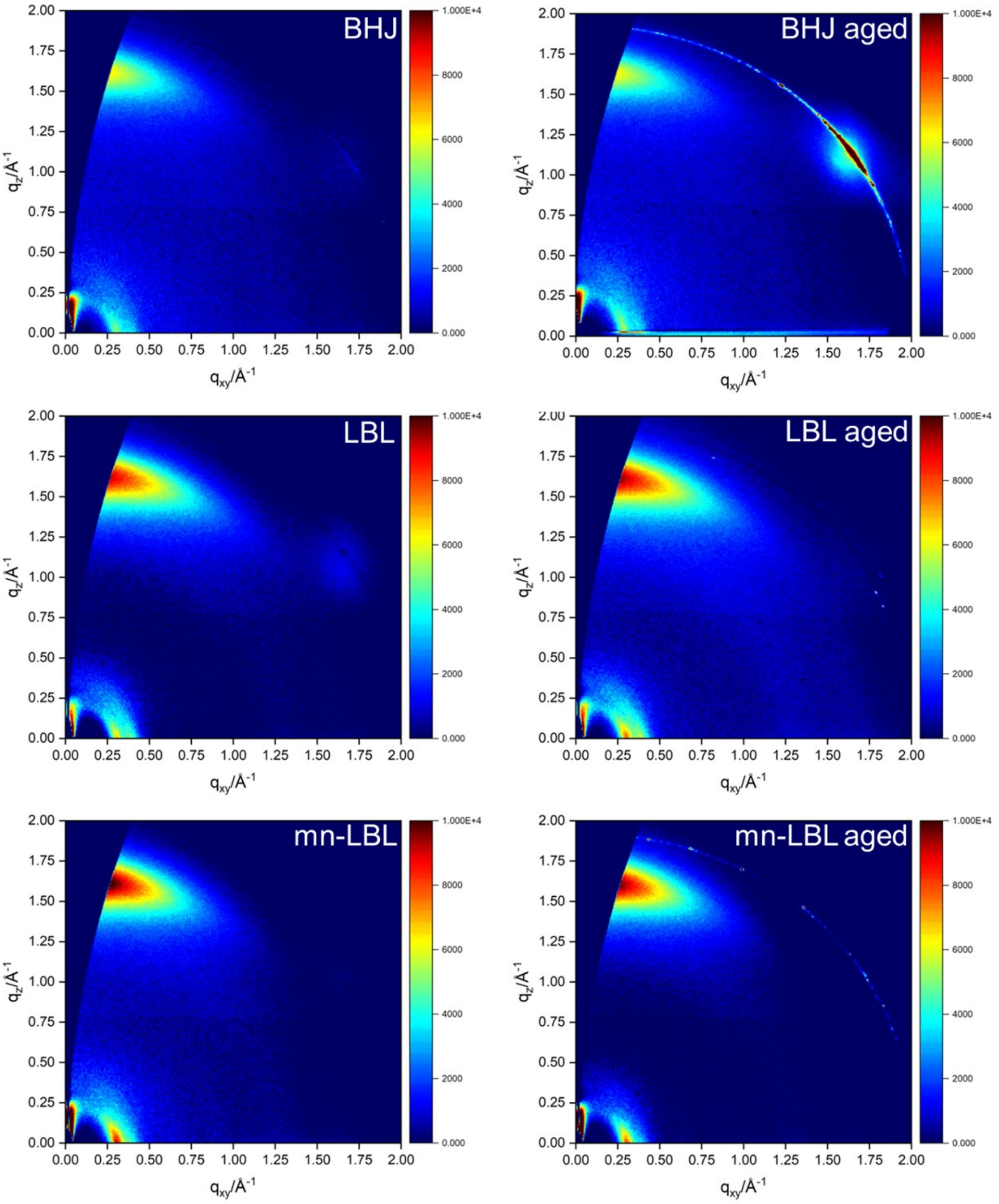

Figure S22. 2D GIWAXS patterns of 250 nm-thick BHJ, conventional LBL and mn-LBL PM6:BTP-eC9 films before and after 1 sun illumination at 85 ºC in N_2 atmosphere for 200 hrs.

Table S4. The peak positions, d-spacings, FWHMs and CCLs of 250 nm-thick BHJ, conventional LBL and mn-LBL PM6:BTP-eC9 films before and after 1 sun illumination at 85 ºC in N_2 atmosphere for 200 hrs.

Film	IP				OOP			
	q (Å^{-1})	d-spacing (Å)	FWHM (Å^{-1})	CCL (Å)	q (Å^{-1})	d-spacing (Å)	FWHM (Å^{-1})	CCL (Å)
BHJ	0.302	20.8	0.164	34.46	1.681	3.738	0.290	19.47
c-LBL	0.302	20.8	0.149	37.96	1.681	3.738	0.291	19.46
mn-LBL	0.302	20.8	0.094	60.32	1.681	3.738	0.281	20.10
BHJ aged	0.302	20.8	0.166	33.94	1.681	3.738	0.289	19.57
c-LBL aged	0.297	21.1	0.152	37.21	1.681	3.738	0.297	19.01
mn-LBL aged	0.302	20.8	0.091	62.21	1.662	3.780	0.272	20.76

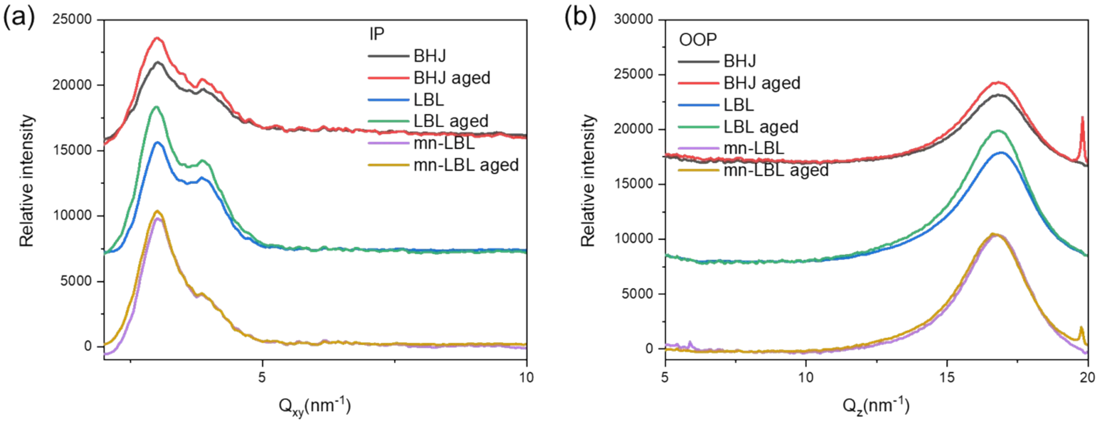

Figure S23. GIWAXS (a) in-plane and (b) out-of-plane line-cuts of 250 nm-thick BHJ, conventional LBL and mn-LBL PM6:BTP-eC9 films before and after 1 sun illumination at 85 ºC in N_2 atmosphere for 200 hrs.

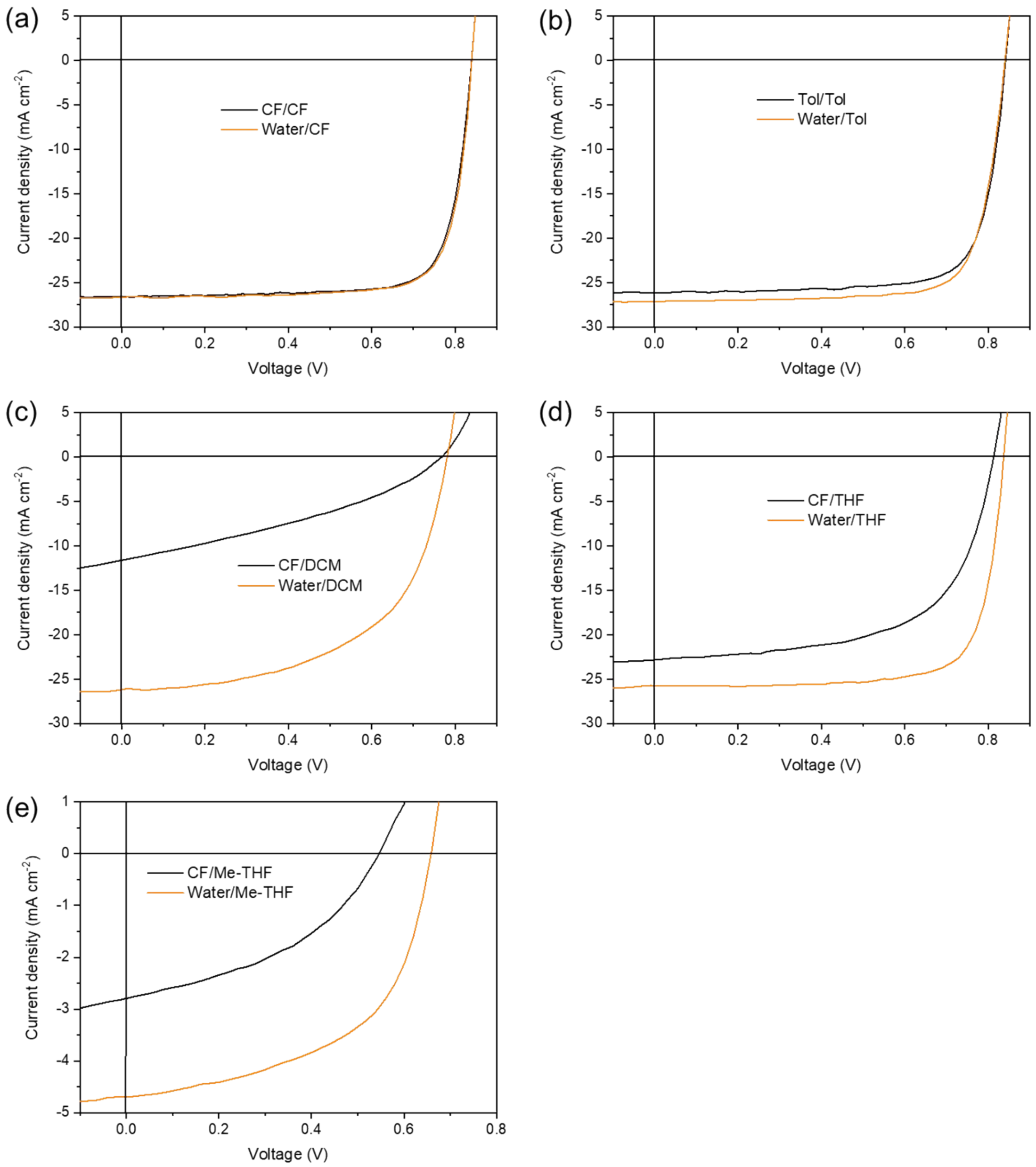

Figure S24. J-V curves of LBL PM6:BTP-eC9 devices processed by (a) chloroform, (b) toluene (c) DCM, (d) THF and (e) Me-THF.

Table S5. Photovoltaic parameters of PM6:BTP-eC9 devices with mn-donor layer processed by different solvents.

Processing solvents	V_{OC} (V)	Jsc (mA cm^{-2})	FF (%)	PCE (%)
CF/CF	0.839	26.55	78.09	17.40 (17.20 ± 0.20)
Water/CF	0.837	26.61	78.49	17.48 (17.21 ± 0.27)
Tol/Tol	0.840	26.18	76.54	16.83 (16.62 ± 0.21)
Water/Tol	0.839	27.18	76.86	17.53 (17.28 ± 0.25)
CF/DCM	0.766	11.61	34.87	3.10 (2.98 ± 0.22)
Water/DCM	0.780	26.19	56.21	11.48 (11.12 ± 0.36)
CF/THF	0.812	22.83	60.84	11.28 (11.00 ± 0.28)
Water/THF	0.839	26.25	76.40	16.83 (16.66 ± 0.25)
CF/Me-THF	0.545	2.79	41.81	0.64 (0.60 ± 0.40)
Water/Me-THF	0.656	4.63	54.20	1.67 (1.21 ± 0.47)

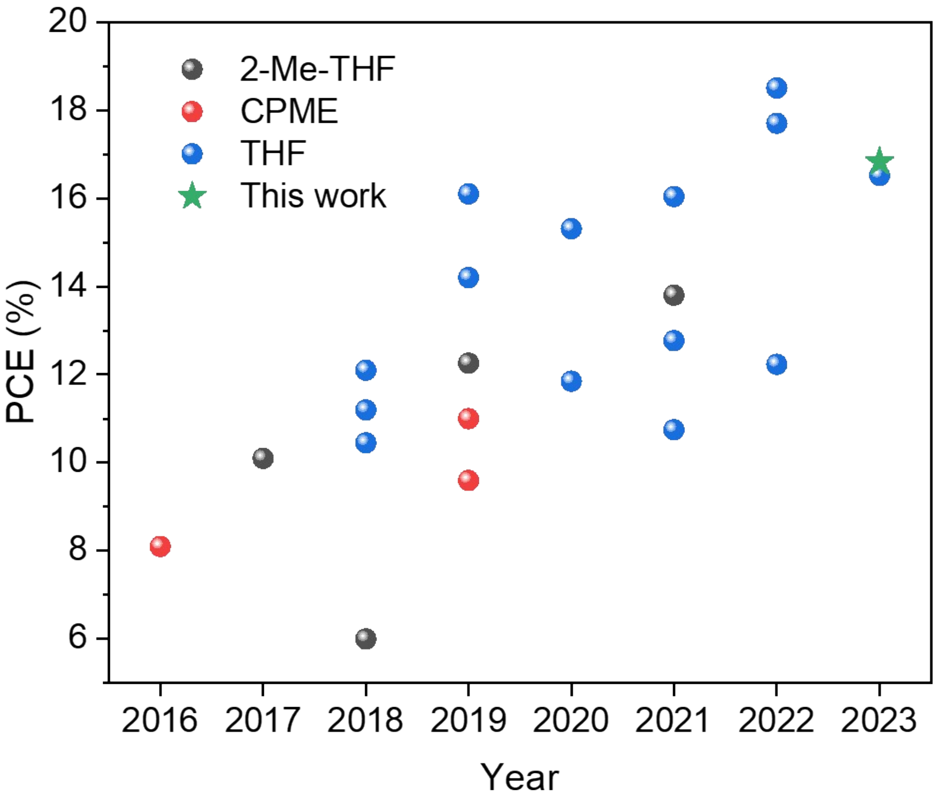

Figure S25. Efficiency evolution of organic solar cells processed by different non-aromatic solvents.

Table S6. Classification of representative OSCs processed by non-aromatic solvents.

NO.	Year	Active layer	Solvent	PCE (%)	URL
1	2016	SPVM1:PC$_{61}$BM	CPME	8.1	https://doi.org/10.1039/c6ta09626c
2	2017	PTzBI-Si:N2200	Me-THF	10.1	https://doi.org/10.1002/adma.201703906
3	2018	PTB7-Th:PDI dimers	Me-THF	6	https://doi.org/10.1002/smtd.201800081
4	2018	PBDB-T-BO/PBDB-BzT:IT-M	THF	12.1	https://doi.org/10.1039/C8TA00368H
5	2018	DRTT-T / DRTT-R:F-2Cl	THF	10.45	https://doi.org/10.1002/adma.201703973
6	2018	BDT3TR-SF:NBDTP-Fout/NBDTP- Fin	THF	11.2	https://doi.org/10.1002/smll.201804271
7	2019	PTB-EDOT/PTB-EDOTS:ITIC-Th	Me-THF	12.26	https://doi.org/10.1039/C8TA10882J
8	2019	PTzBI-Si:N2200	CPME	11	https://doi.org/10.1039/C8EE02863J
9	2019	J51:PTB7-Th:N2200	CPME	9.6	https://doi.org/10.1021/acsami.9b06963
10	2019	PBDB-TF-T1:BTFP-4F-12	THF	16.1	https://doi.org/10.1002/adma.201903441
11	2019	T1: IT-4F	THF	14.2	https://doi.org/10.1002/adma.201808356
12	2020	PTQ10:HO-IDIC-2F	THF	11.85	https://doi.org/10.1039/D0TC01313G
13	2020	PM6-Ir1.5:Y6-C2	THF	15.31	https://doi.org/10.1002/solr.202000156
14	2021	PTzBi-OF:PS1	Me-THF	13.8	https://doi.org/10.1039/D0CC07213C
15	2021	PTB7-Th: BTPV-4F-eC9	THF	12.77	https://doi.org/10.1002/adfm.202102361
16	2021	PE25: Cl-BTA	THF	10.75	https://doi.org/10.1021/acsami.1c14317
17	2021	PBDTTPD-HT:BTP-2F-BO	THF	16.04	https://doi.org/10.1016/j.xcrp.2021.100517
18	2022	PBDB-T-b-PYT	THF	12.23	https://doi.org/10.1002/solr.202101024
19	2022	PM1:L8-BO	THF	17.7	https://doi.org/10.1039/D2EE03134E
20	2022	PM1:L8-BO:BTP-F3Cl	THF	18.5	
21	2023	SSC-T1:N3	THF	16.52	https://doi.org/10.1016/j.nanoen.2022.108059

22	2023	PM6:BTP-eC9	THF	16.83	This work

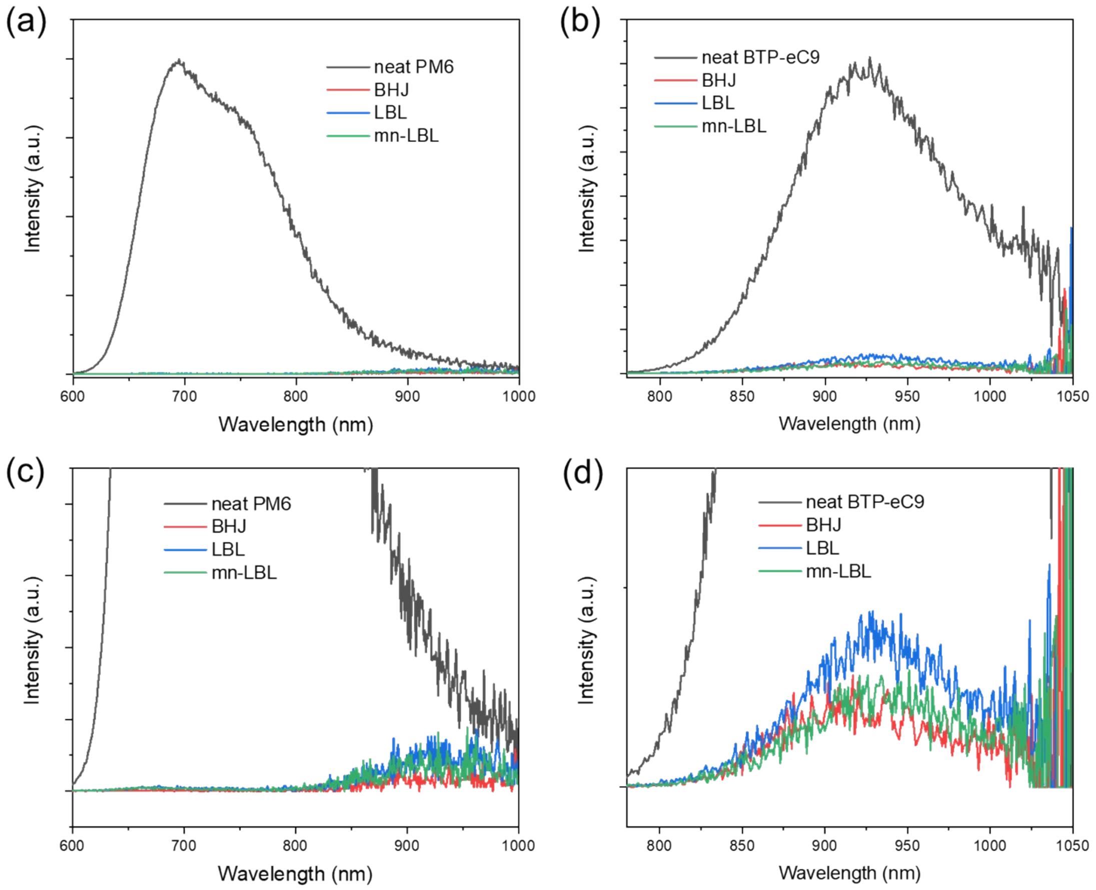

Figure S26. Steady-state PL spectra of 250 nm-thick BHJ, conventional LBL and mn-LBL PM6:BTP-eC9 films excited at (a,c) 560 nm and (b,d) 750 nm.

Table S7. PL lifetime of different films

Film	Lifetime	
	Probe @670nm	Probe @930nm
PM6 only	547 ps	-
BTP-eC9 only	-	1434 ps
BHJ	106 ps	382 ps
LBL	119 ps	411 ps
mn-LBL	104 ps	310 ps

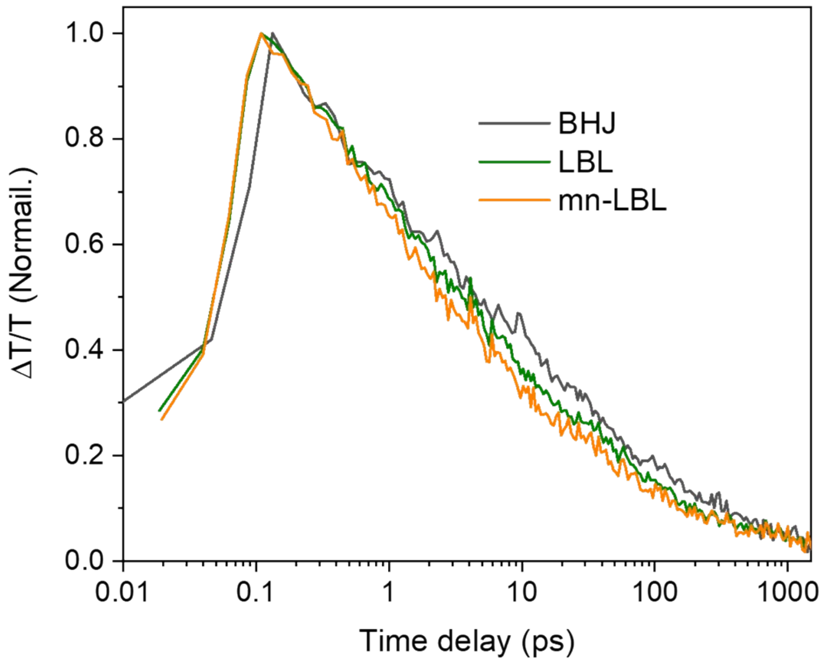

Figure S27. Fs-TA decay dynamics probed at 825 nm of PM6:BTP-eC9 films processed by BHJ, c-LBL and mn-LBL techniques.

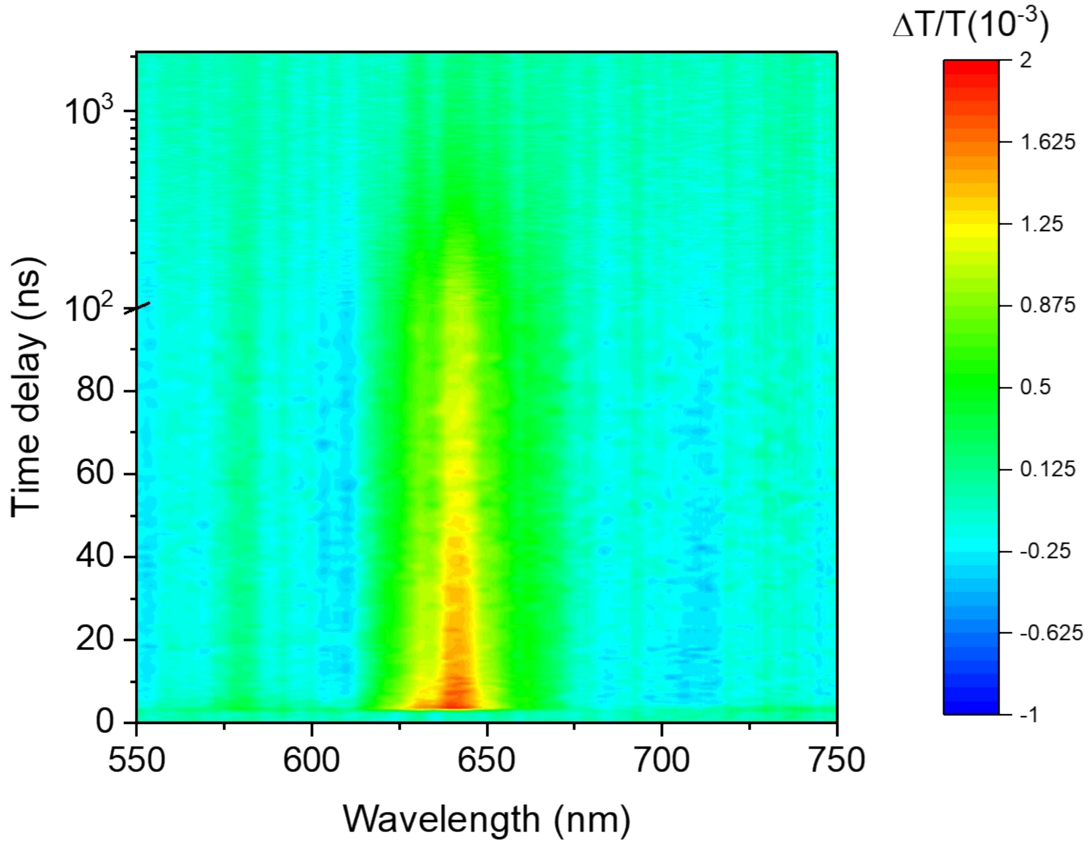

Figure S28. 2D ns-TA contour of PM6:BTP-eC9-based mn-LBL films.

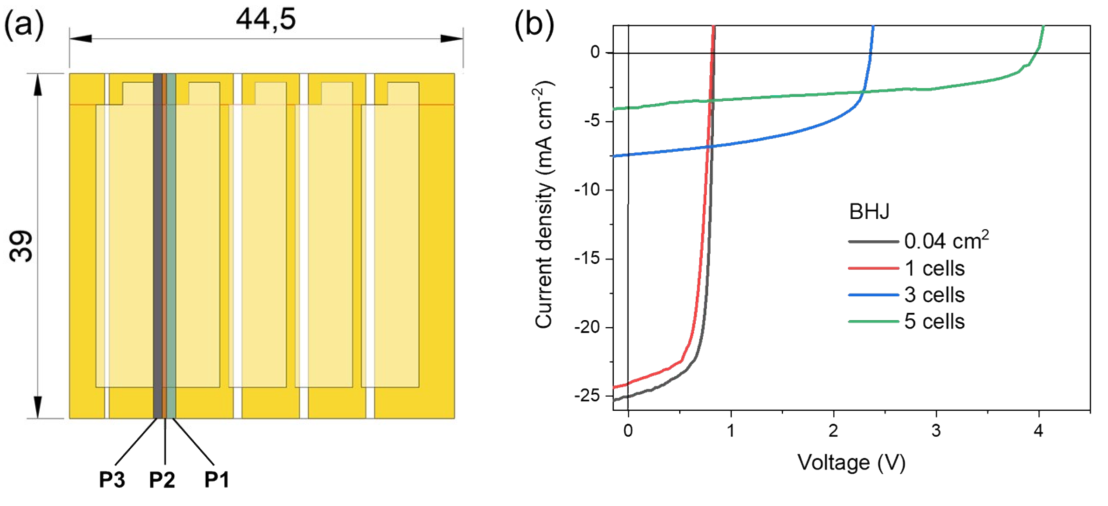

Figure S29. (a) Module device design and (b) J-V curves of BHJ modules processed by PM6:BTP-eC9 blend solution.

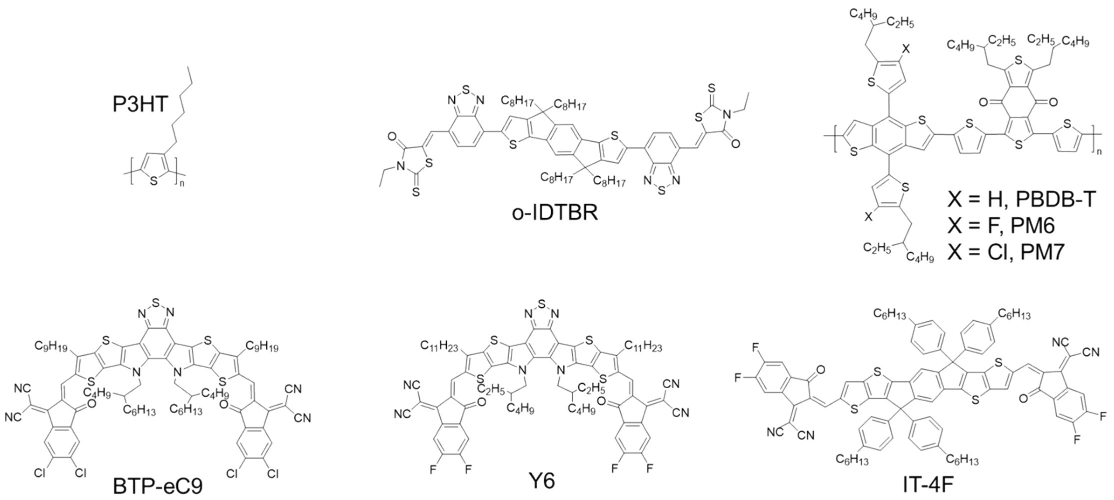

Figure S30. Chemical structure of donor and acceptors for universality test of mn-LBL processing of OSCs

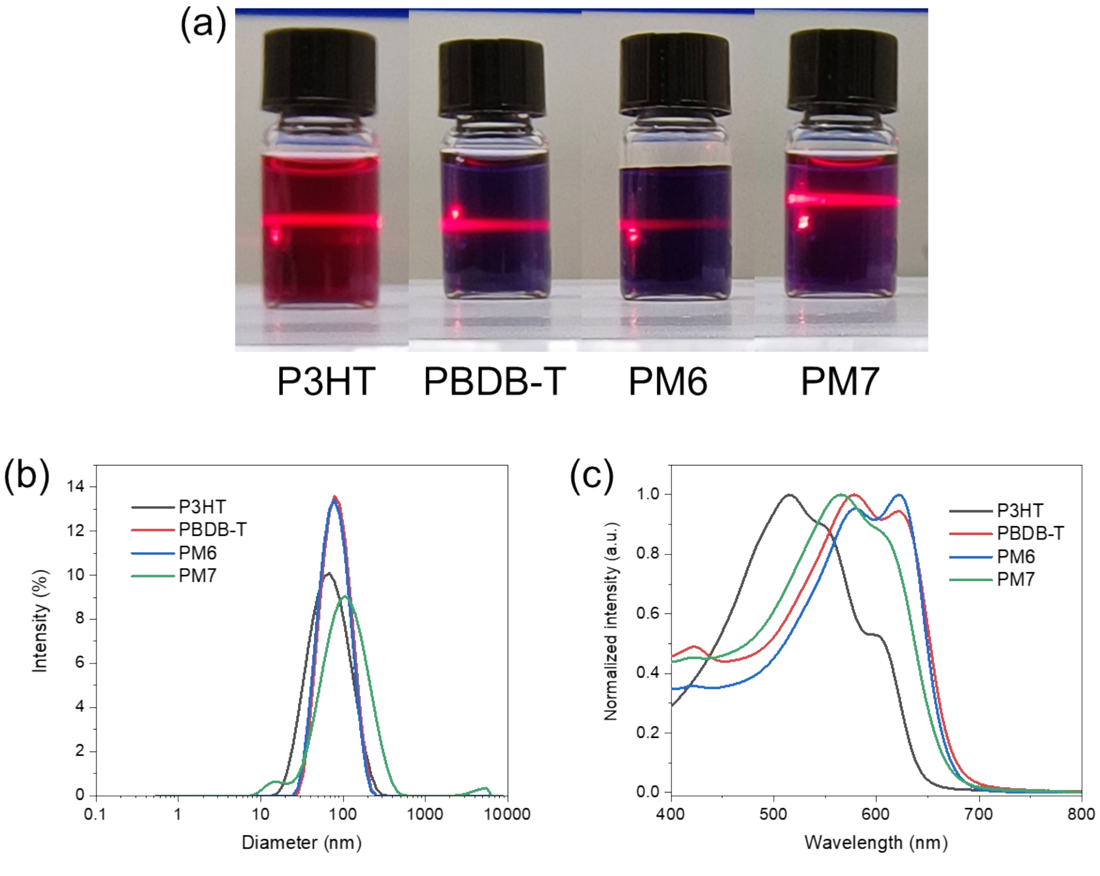

Figure S31. (a) Tyndall effect observed from different polymer NP dispersion. (b) NP size distribution detected by DLS. (c) UV–vis absorption spectra of NP inks.

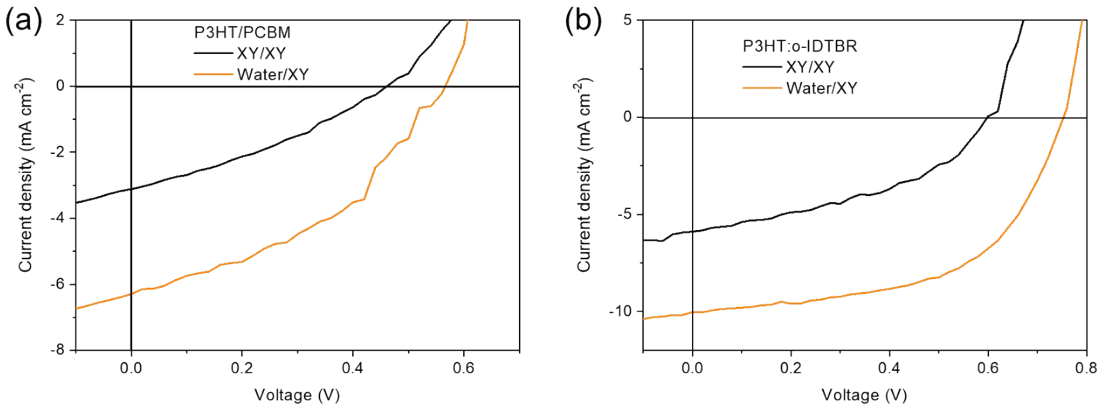

Figure S32. J-V curves of LBL (a) P3HT:PCBM and (b) P3HT:o-IDTBR devices.

Table S8. Photovoltaic parameters of P3HT:PCBM and P3HT:o-IDTBR devices processed by different solvents.

Acceptor	Processing solvents	Voc (V)	Jsc (mA cm^{-2})	FF (%)	PCE (%)
PCBM	XY/XY	0.461	3.12	32.01	0.46
	Water/XY	0.563	6.29	40.42	1.43
o-IDTBR	XY/XY	0.602	5.90	41.29	1.47
83	Water/XY	0.753	10.04	55.59	4.20

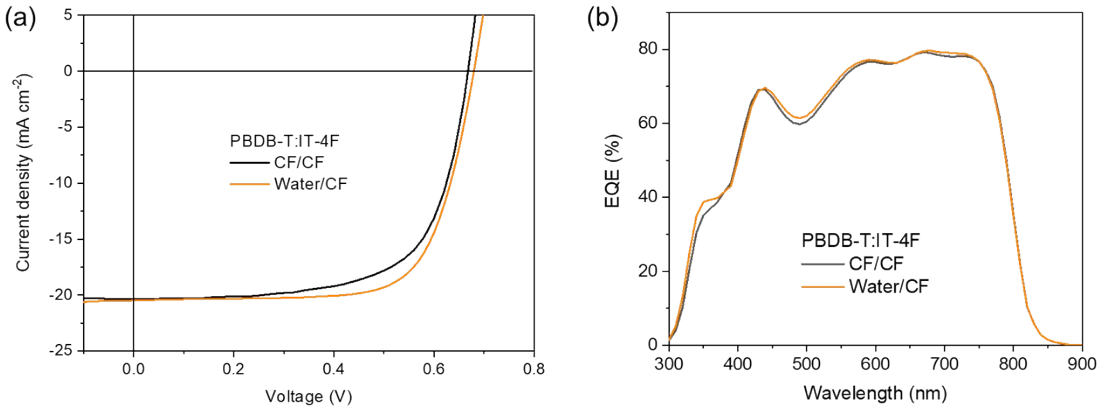

Figure S33. (a) J-V curves and (b) EQE spectra of PBDB-T: IT-4F devices prepared by LBL technique with different solvents.

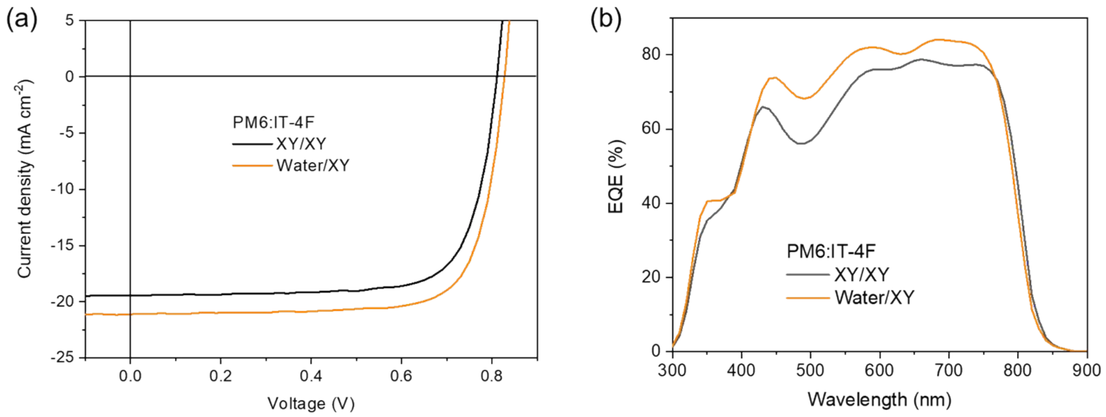

Figure S34. (a) J-V curves and (b) EQE spectra of PM6: IT-4F devices prepared by LBL technique with different solvents.

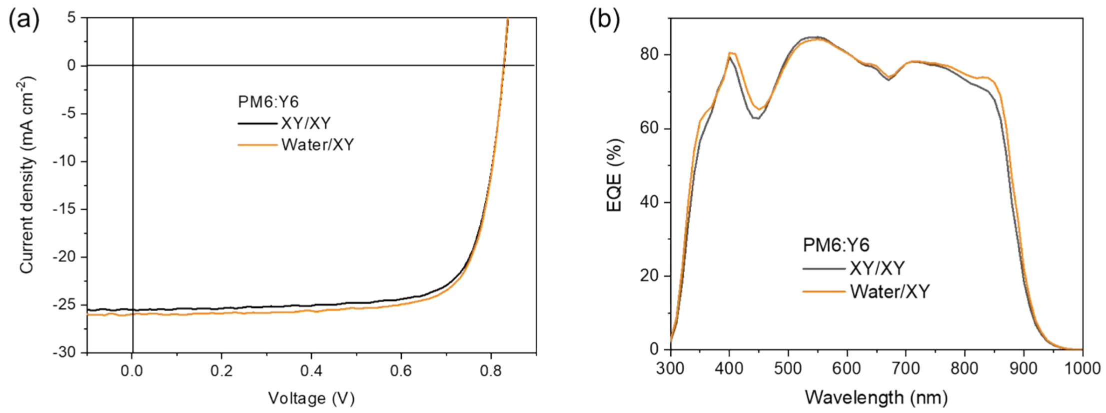

Figure S35. (a) J-V curves and (b) EQE spectra of PM6: Y6 devices prepared by LBL technique with different solvents.

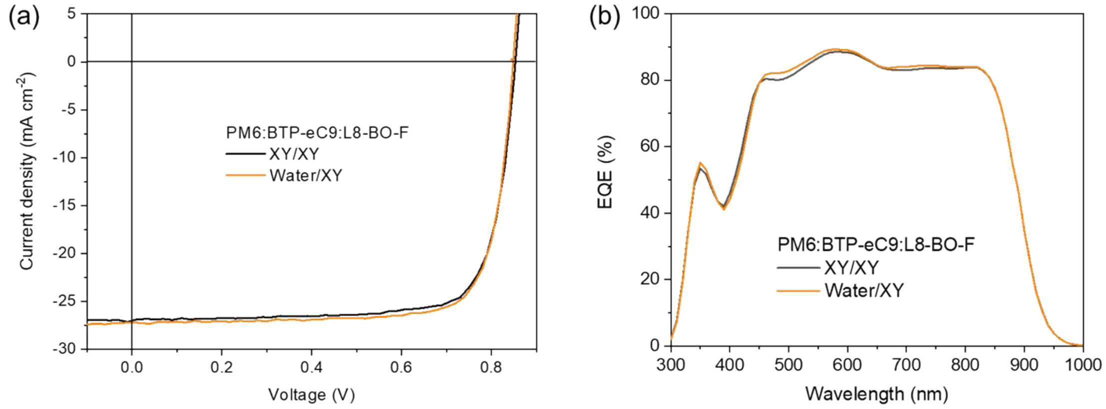

Figure S36. (a) J-V curves and (b) EQE spectra of PM6: BTP-eC9:L8-BO-F devices prepared by LBL technique with different solvents.

Table S9. Photovoltaic parameters of LBL-processed devices with various active layer materials.

Materials	Processing solvents	Voc (V)	Jsc (mA cm^{-2})	Jsc^{a} (mA cm^{-2})	FF (%)	PCE^{b} (%)
PBDB-T/IT-4F	CF/CF	0.666	20.35	19.30	66.56	9.02 (8.90 ± 0.12)
	Water/CF	0.680	20.44	19.45	71.02	9.87 (9.79 ± 0.10)
PM6:IT-4F	XY/XY	0.809	19.45	19.25	75.35	11.86 (11.63 ± 0.23)
	Water/XY	0.825	21.11	20.65	76.28	13.28 (13.01 ± 0.27)
PM6:Y6	XY/XY	0.828	25.50	24.75	76.16	16.07 (15.90 ± 0.17)
	Water/XY	0.827	25.95	25.22	76.62	16.43 (16.20 ± 0.23)
PM6:BTP-eC9:L8-BO-F	XY/XY	0.847	27.02	26.98	78.95	17.95 (17.90 ± 0.23)
	Water/XY	0.856	27.28	27.16	79.33	18.33 (18.04 ± 0.29)

[a] Calculated from EQE.

[b] Average values with standard deviation were obtained from 15 devices.

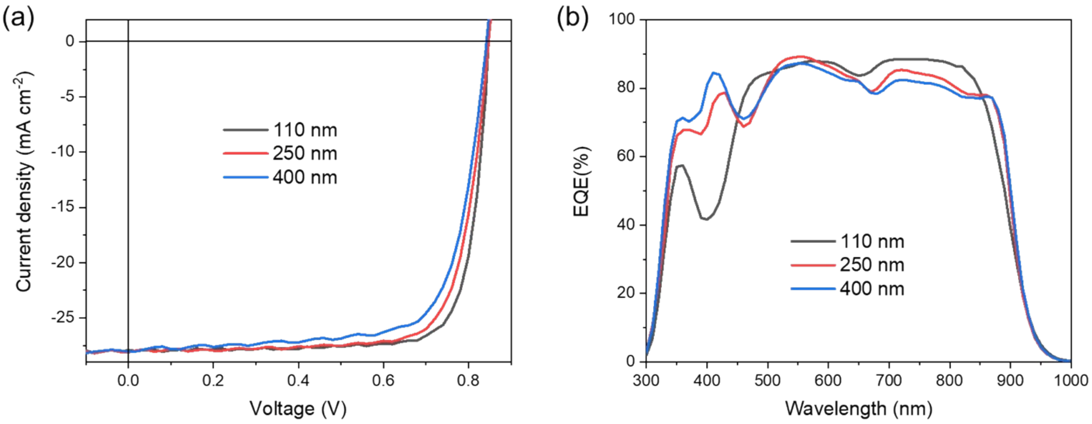

Figure S37. (a) J-V curves and (b) EQE spectra of thickened PM6: BTP-eC9 devices with additive DTT prepared by mn-LBL technique.

Table S10. Photovoltaic parameters of PM6: BTP-eC9:L8-BO-F devices prepared by mn-LBL technique with different thicknesses.

Thickness (nm)	V_{OC} (V)	J_{SC} (mA cm^{-2})	$J_{SC}{}^{a}$ (mA cm^{-2})	FF (%)	PCE^{b} (%)

110 ± 10	0.846	27.92	27.47	80.49	19.01 (18.61 ± 0.39)
250 ± 20	0.846	28.10	27.57	76.53	18.19 (18.01 ± 0.21)
400 ± 20	0.841	28.07	27.41	73.02	17.22 (16.98 ± 0.26)

[a] Calculated from EQE;

[b] Average values with standard deviation were obtained from 20 devices;

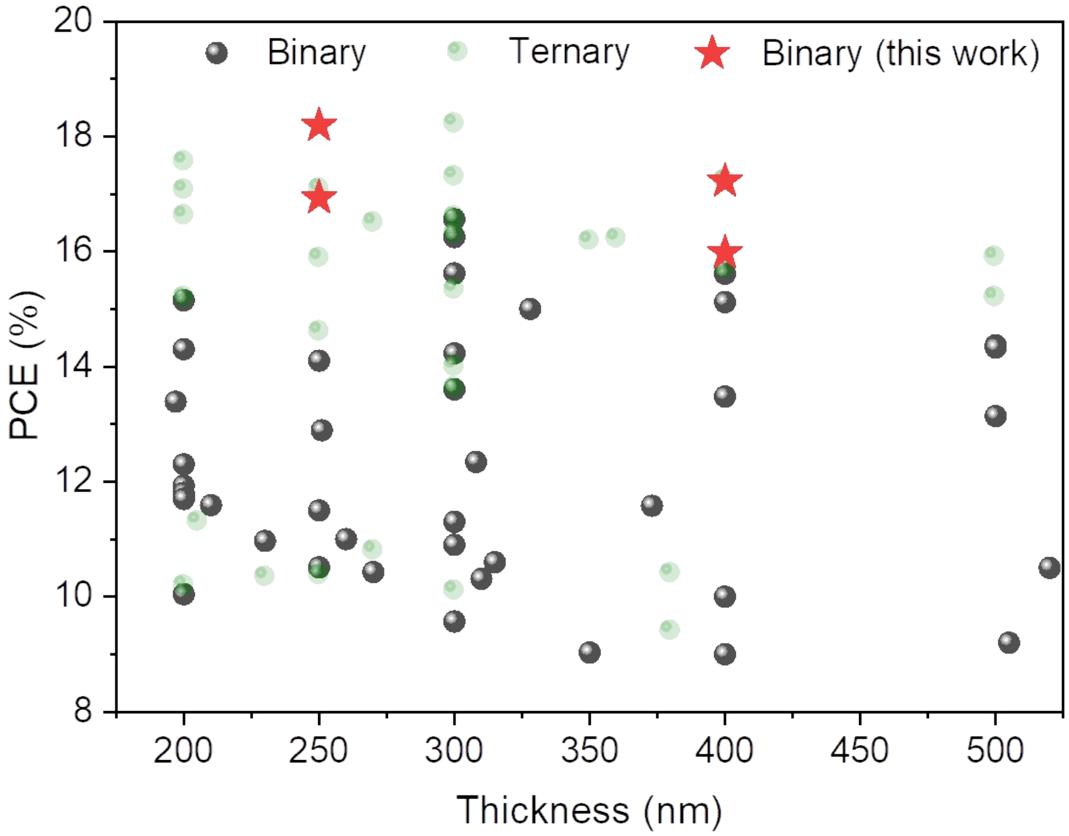

Figure S38. Plots of the PCE versus active layer thickness for binary and ternary OSCs.

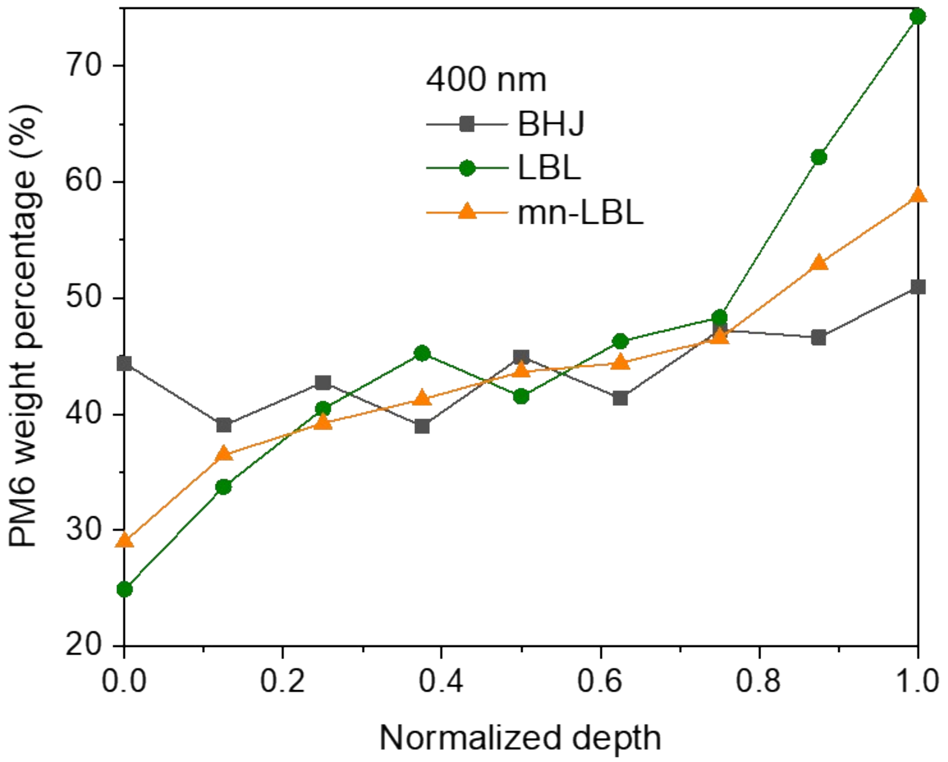

Figure S39. PM6 weight content throughout the entire active layer of 400 nm-thick PM6:BTP-eC9 films.

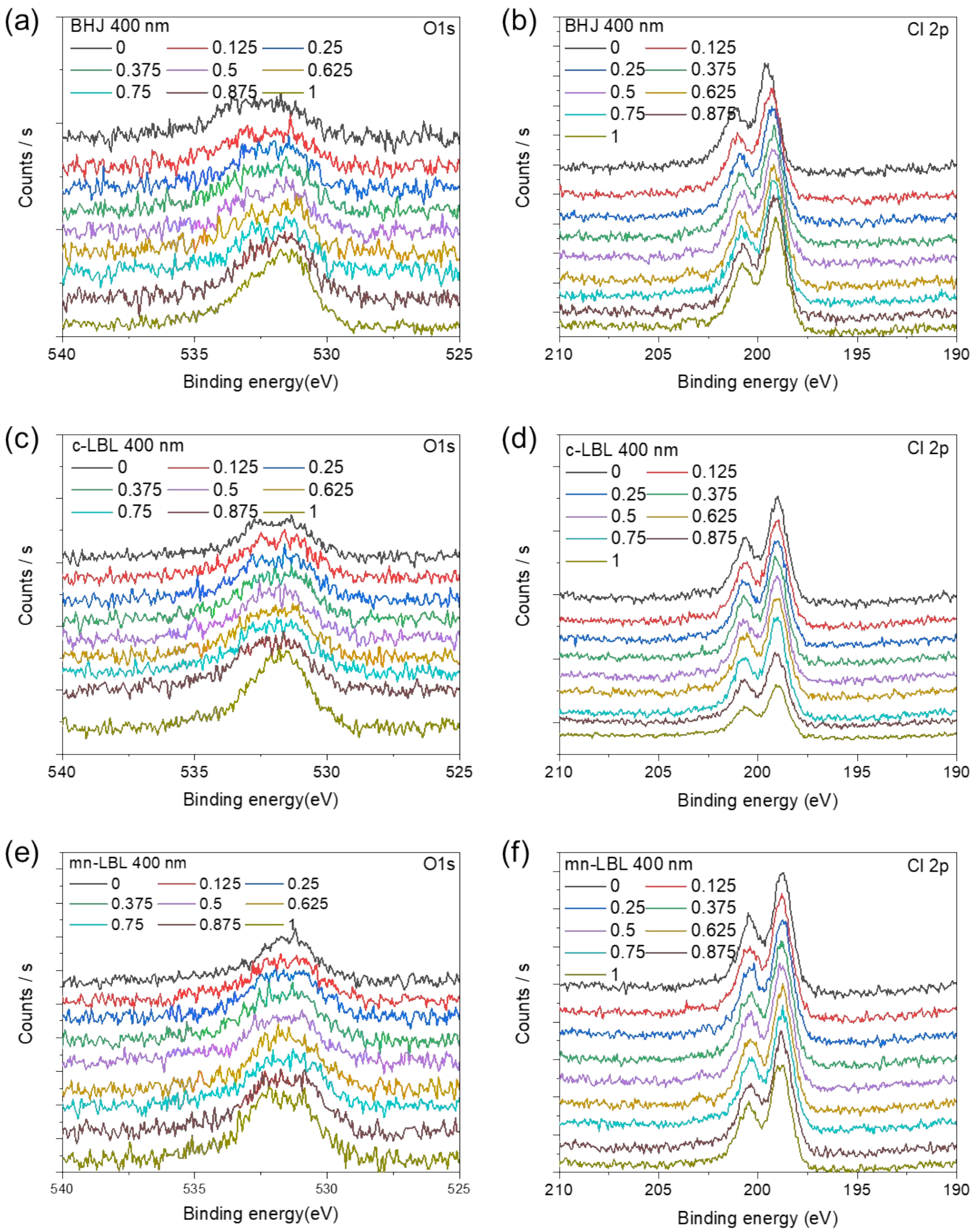

Figure S40. XPS scans as a function of normalized depth of 400 nm-thick PM6:BTP-eC9 films processed by (a,b) BHJ, (c,d) c-LBL and (e.f) mn-LBL techniques in the (a,c,e) O1s and (b,d,f) Cl2p binding regions.

References

1 P. W. M. Blom, M. J. M. De Jong and J. J. M. Vleggaar, *Appl. Phys. Lett.*, 1996, **68**, 3308–3310.

2 C. Xie, A. Classen, A. Späth, X. Tang, J. Min, M. Meyer, C. Zhang, N. Li, A. Osvet, R. H. Fink and C. J. Brabec, *Adv. Energy Mater.*, 2018, **8**, 1702857.

3 Y. Zhang, D. Deng, Z. Wang, Y. Wang, J. Zhang, J. Fang, Y. Yang, G. Lu, W.

Ma and Z. Wei, *Adv. Energy Mater.*, 2017, **7**, 1701548.

4 L. Bu, S. Gao, W. Wang, L. Zhou, S. Feng, X. Chen, D. Yu, S. Li and G. Lu, *Adv. Electron. Mater.*, 2016, **2**, 1600359.

5 Y. Zhang, H. Feng, L. Meng, Y. Wang, M. Chang, S. Li, Z. Guo, C. Li, N. Zheng, Z. Xie, X. Wan and Y. Chen, *Adv. Energy Mater.*, 2019, **9**, 1902688.